Phenomenology of polarised Cross Sections for $W^{\pm}Z$ in Sherpa

Bachelor-Arbeit
zur Erlangung des Hochschulgrades
Bachelor of Science
im Bachelor-Studiengang Physik

vorgelegt von

Jannes Liersch
geboren am 18.11.2000 in Cottbus

Institut für Kern- und Teilchenphysik
Fakultät Physik
Bereich Mathematik und Naturwissenschaften
Technische Universität Dresden

2022

Eingereicht am 20. Dezember 2022

1. Gutachter: Dr. Frank Siegert
2. Gutachter: Prof. Dr. Dominik Stöckinger

Abstract

English:
Studying the polarisation of weak bosons provides crucial insights into the mechanism of electroweak symmetry breaking. An implementation of polarised cross sections in Sherpa using the narrow-width approximation will be studied by comparing its results to the cross sections and distributions of selected kinematic variables obtained by PHANTOM using double-pole approximation. For this purpose, the $W^{\pm}Z$ inclusive production process is investigated with the help of the analysis tool Rivet. Results for different kinematic observables are discussed for all possible pol combinations with the polarisation defined in different reference frames.

Deutsch:
Die Untersuchung der Polarisation von Bosonen der schwachen Wechselwirkung kann entscheidende Einsichten über den Mechanismus der elektroschwachen Symmetriebrechung liefern. Eine Implementierung von polarisierten Wirkungsquerschnitten in Sherpa unter Verwendung der Narrow-Width Näherung wird untersucht indem ihre Ergebnisse mit den Wirkungsquerschnitten und Verteilungen ausgewählter kinematischer Variablen verglichen werden, die mit PHANTOM unter Verwendung der Double-Pole Näherung erhalten wurden. Zu diesem Zweck wird der inklusive $W^{\pm}Z$ Produktionsprozess mit Hilfe des Analyseprogramms Rivet untersucht. Die Ergebnisse werden für verschiedene kinematische Observablen für alle möglichen Polarisationen mit der in verschiedenen Bezugssystemen definierten Polarisation diskutiert.

Contents

1 Introduction **1**

2 Theoretical Background **3**

2.1 Introduction to Particle Physics . . . 3

2.2 Symmetry Breaking and Electroweak Gauge Theory . . . 5

2.3 Polarisation . . . 7

2.4 LHC and Proton-Proton Collisions . . . 9

2.4.1 Scattering Parameters . . . 10

2.5 W^+Z Production . . . 11

3 Simulation and Analysis Framework **15**

3.1 Monte Carlo Event Generators . . . 15

3.2 Polarisation in Event Generators . . . 17

3.2.1 Narrow Width Approximation . . . 18

3.2.2 Double Pole Approximation . . . 18

3.3 Data Analysis with Rivet . . . 19

4 Simulation, Analysis and Results **21**

4.1 Simulation Configuration . . . 21

4.2 Rivet Analysis . . . 23

4.3 Study of Generated Events . . . 24

4.3.1 Integrated Cross Sections . . . 24

4.3.2 Distributions . . . 26

5 Summary and Outlook **35**

A Appendix **37**

A.1 SHERPA Full Process Runcard . . . 37

A.2 SHERPA Polarised Process Runcard . . . 39

A.3 Rivet Analysis . . . 41

A.4 SHERPA Feynman Graph Output . . . 46

A.5 Muon Decay Angle for right- and left-handed Modes . . . 47

B Bibliography 49

Acronyms

BSM Beyond Standard Model physics. 9

CM Centre-of-Mass frame. 9, 24–33

DPA Double Pole Approximation. 18, 23–30, 32, 33

dXS differential cross section. 12, 26, 28

LAB Laboratory frame. 9–11, 24–26, 28, 30–33

LL Longitudinally polarised W^+ boson and Longitudinally polarised Z boson. 25, 28

LO Leading Order. 19, 24, 26, 28

LT Longitudinally polarised W^+ boson and Transversely polarised Z boson. 28, 31

NLO Next-to Leading Order. 17, 19, 21, 24, 26, 28, 31

NWA Narrow Width Approximation. 18, 21, 23, 25–30, 32, 33

QCD Quantum Chromo Dynamics. 9

QED Quantum Electrodynamics. 15

Sherpa Simulation of High-Eenergy Reactions of Particles. iii, 11, 15, 18, 19, 21–26, 35

SM Standard Model of Particle Physics. 1, 3–7, 9, 15

TL Transversely polarised W^+ boson and Longitudinally polarised Z boson. 28, 31

TT Transversely polarised W^+ boson and Transversely polarised Z boson. 25, 28

XS cross section. 12, 13, 24, 25, 27

1 Introduction

The concept of matter consisting, at its smallest scale, of fundamental, indivisible particles can be traced back as far as the 8th century BCE when basic instances of atomism were developed by Indian philosophers[1] and Greek philosophers followed in the 5th century BCE. [1] It should take over 2600 years to experimentally prove the existence of a particle that to this day could not be proven to be dividable. This particle, the electron, was experimentally proven by J.J. Thomson in 1897. [2]

Although a range of fundamental particles was found by particle colliders, detectors and similar experiments over the last 125 years, the Standard Model does not provide a full explanation of our universe. This led to the search and development of Beyond Standard Model Physics (BSM), either in form of an extension of the SM or fundamentally new models. The newest addition to the SM is the Higgs boson, found at the particle collider LHC in 2012[3]. However, experimental results that would favour proposed alternatives to the SM have yet to be found. A way of testing the SM is the search for deviations from the predicted outcomes. By precisely measuring the properties of particles and their interactions, physicists hope to find to find deviations from the SM prediction, leading to BSM physics. A group of processes that might be sensitive to new physics is vector boson pair (VB) production. The longitudinal polarisation of VBs is a direct consequence of the electroweak symmetry breaking, making them especially sensitive to deviations from SM in the electroweak sector.

By performing simulations and comparing with and predicting experimental results one can probe the underlying theory of polarisation. The ability to simulate polarised bosons is currently being implemented in Sherpa, a widely used Monte-Carlos-Event generator for simulating high-energy physics. This implementation is currently being verified by comparing with previous literature results. The goal of this thesis is to investigate a process that has not yet been validated, the $W^{\pm}Z$ pair production.

This work aims to explain the basic concepts that are needed to understand the conducted tests and comparisons. Therefore, chapter one will explain the Standard Model of Particle Physic, Electroweak Symmetry Breaking, Polarisation, the LHC with its collisions and the $W^{+}Z$ process. Chapter three reviews the used simulation and analysis framework, including Monte Carlo Event Generators, the Data Analysis with Rivet and the output Feynman Diagrams. Chapter 4 describes the settings and results of the simulation and analysis. Summarizing the obtained results will be done in Chapter 5.

2 Theoretical Background

2.1 Introduction to Particle Physics

Particle Physics is the field of physics that investigates the smallest known particles and their interactions. Particles may interact in one of four ways: gravitational, electromagnetic, weak or strong. These are called fundamental forces. They are gravity, electromagnetic, weak, and strong force. The classical idea of forces and fields needs to be modified at a small scale to accommodate quantum effects. As a solution, each force has one or multiple mediators. Interactions happen by exchanging these mediators between the particles that make up matter. Mediators cannot be observed directly, resulting in the term virtual particles.
Gravity describes the phenomenon of bodies with mass being drawn to each other and is the weakest of the fundamentals but has the longest range. Its hypothetical mediator particle is called the graviton.
Electromagnetic forces describe the interaction of particles that have a property called electric charge. Lightning is a phenomenon caused by this force. The mediator is the photon.
Weak interaction has a short range and three mediators, the W^+, W^-, and the Z boson. Radioactivity can be explained by this force.
Strong or nuclear interaction is the force with the highest relative strength. It binds neutrons and protons to atoms and has 8 mediators, the gluons.[4, 5]
At this point, physicists have managed to unify all but one force into one theory. Gravity cannot yet be included in the current leading theory, the Standard Model of Particle Physics (SM). Therefore, the SM differentiates between 13 different mediators: one photon, three massive bosons, eight gluons, and the Higgs boson. The latter is the mediator for the Higgs field, this will be discussed in section 2.2.

The SM is the most widely accepted and well-tested theory and uses 18, depending on the interpretation, fundamental particles to describe everything happening in our universe. It fails to explain dark matter, dark energy and some other phenomena. Therefore, the SM in its current state is obviously not yet the theory of everything. It is however the best-known explanation that Physicists have been able to verify experimentally. The SM is formulated as a gauge quantum field theory with a local gauge symmetry: $SU(3)_C \times SU(2)_L \times U(1)_Y$. Every Lagrangian has to be invariant under this symmetry, where, for each $n \geq 1$, $SU(n)$ is

the Special Unitary Group, the group of n-dimensional complex unitary matrices under multiplication with determinant 1.
Using Noether's theorem [4], each symmetry receives a conserved quantity: electric charge, the third component of the weak isospin and the strong charge or colour charge. For the strong interaction, the gauge symmetry is the $SU(3)$ subgroup. If the forces are separated, this is called Quantum Chromo Dynamics (QCD). The $SU(2) \times U(1)$ is called the electroweak subgroup and is used to describe the union of the electromagnetic and weak interaction.

Particles are distinguished by their attributes. Additionally to the three charges, there are mass and spin. Using the spin, the particles can be divided into two categories. Particles with half-integer spin are called fermions since they have anticommuting statistics[5]. Fermions make up all massive particles. In particular, protons, neutrons and electrons are themselves fermions or made up of fermions and make up all matter in the universe. Even-integer spin particles mediate forces that are either repulsive or attractive, while odd-integer ones are both attractive and repulsive. Experimental results suggest that $W^{\pm}, Z$ bosons, gluons, and the photon have integer spin. Thus, the three SM forces are repulsive and attractive. The graviton would have a spin of two since gravity is only attractive. Similarly, Higgs boson has spin zero.[6]

Fermions can be divided into three different groups or generations. The first generation are the particles that make up the matter in our everyday lives, so electrons, up quarks, and down quarks. The electron neutrino is also part of this category. The second and third generations are made up out of particles with the same attributes as their counterparts in the first generation, but with increasing mass per generation. This can be seen in figure 2.1
Fermions are also differentiated by their charges and thereby the interactions they can take part in. If it is possible for them to interact in all three ways they are named quarks. Consequently, they have an electric charge, a colour charge and a third component of the weak

	Leptons				Quarks			
	Particle		Q	mass/GeV	Particle		Q	mass/GeV
First generation	electron	(e^-)	-1	0.0005	down	(d)	$-1/3$	0.003
	neutrino	(ν_e)	0	$< 10^{-9}$	up	(u)	$+2/3$	0.005
Second generation	muon	(μ^-)	-1	0.106	strange	(s)	$-1/3$	0.1
	neutrino	(ν_μ)	0	$< 10^{-9}$	charm	(c)	$+2/3$	1.3
Third generation	tau	(τ^-)	-1	1.78	bottom	(b)	$-1/3$	4.5
	neutrino	(ν_τ)	0	$< 10^{-9}$	top	(t)	$+2/3$	174

Figure 2.1: The three generations of fermions, divided into quarks and leptons.[4]

isospin. Leptons, on the other hand, cannot interact via the strong force. Further, they have an integer electric charge while quarks only possess electric charges of multiples of $\frac{1}{3}$. However, this cannot be observed directly due to a phenomenon of the strong interaction called confinement. Due to this, quarks can only exist in states with a neutral colour charge configuration, which results in integer electric charges of the configurations, e.g. protons and neutrons.
The last category of interactions is given by neutrinos, a subgroup of the leptons. Each charged lepton has an assigned neutrino. They do not interact through strong or electromagnetic interaction, but only through weak interaction. This absence of interaction possibilities makes neutrinos the hardest group to detect.
The antiparticle corresponding to a particle has identical mass, but otherwise opposite signed quantum numbers. Every fermion and most bosons have corresponding antiparticles. The only exceptions are the Z-boson and the photon. This leaves us with 24 fermions and 13 bosons.
This sums up the model that describes what we observe and has not been disproved by any experiment yet. However, there are a few parameters that have to be determined experimentally for predictions to be made:

Mass of all fermions	12
Coupling constants	4
Mixing angles	8
Higgs mass and coupling	2

Table 2.1: Standard Model Parameters

Using the SM and General Relativity with these 26 parameters added we can predict any process in particle physics. The exact values of some parameters have not yet been determined and are the subject of ongoing research.

2.2 Symmetry Breaking and Electroweak Gauge Theory

Experiments concluded that $W^{\pm}$- and Z-boson, unlike the photon, have a mass, of around 80 GeV for the $W^{\pm}$-boson and around 91 GeV for the Z-boson. The photon has to be massless in order to not break the $U(1)$ symmetry. Massless gauge bosons have two possible polarisation options, while massive spin-1 particles have three. The missing longitudinal polarisation of the spin-1 $W^{\pm}$- and Z-boson can only be implemented by adding three degrees of freedom to the electroweak symmetry gauge Lagrangian to keep the gauge invariance unbroken. The SM adds a doublet of complex scalar fields:

$$\phi(x) \equiv \begin{pmatrix} \phi^{(+)}(x) \\ \phi^{(0)}(x) \end{pmatrix} = \exp\{\frac{i}{v}\vec{\sigma} \cdot \vec{\phi}(x)\}\frac{1}{\sqrt{2}}\begin{bmatrix} 0 \\ v + H(x) \end{bmatrix} \tag{2.1}$$

Additionally to that, we add a potential to the Lagrangian. This generates the needed electroweak symmetry breaking.

$$\mathcal{L} = (D^\mu)^\dagger D_\mu \Phi - \lambda(|\Phi|^2 - \frac{v^2}{2})^2 \tag{2.2}$$

It makes sense to choose $\lambda > 0$, since the potential should have a lower bound. The covariant derivative

$$D_\mu \Phi = [\partial_\mu + \frac{i}{2} g\vec{\sigma} \cdot \vec{W}_\mu + ig' y_\phi B_\mu]\Phi \tag{2.3}$$

is the coupling operator to connect the scalar doublet to the SM gauge bosons. $y_\phi = \frac{1}{2}$ is the scalar hypercharge, the difference between the weak isospin's third component and the electromagnetic charge. It is conserved by the photon's gauge field $A^\mu(\mathrm{x})$, not coupling to $\phi^{(0)}$, while $\phi^{(+)}$ has to have the fitting electric charge. Consequently, the neutral scalar field doesn't interfere with the electric charge and therefore can acquire a vacuum expectation value. The number of possible minimum energies is infinite, but by a choosing certain ground state, e.g. $\vec{\varphi} = H = 0$ in $\Phi(x)$, the symmetry breaks spontaneously:

$$SU(2)_L \times U(1)_Y \rightarrow U(1)_{EM} \tag{2.4}$$

Jeffrey Goldstone showed that the breaking of continuous global symmetries will always be resulting in one or more massless scalar particles. In our case, three of such particles will appear since the symmetry group had three generators. These bosons can be seen as excitations of the field in the broken symmetries directions and are massless if the symmetries are only broken spontaneously but not explicitly. The excitations in the field do happen on the minimum energy since these are the chosen ground states. This results in the excitation having no energy costs and thereby being massless. [7, 8]
By expanding the gauge field equation about the ground state we see that the gauge field acquires a mass $m_B = \frac{\mu g_Y}{\lambda}$. This leads to the exchange of Goldstone bosons to massive longitudinal polarised bosons and leaves us with a massive gauge field with three degrees of freedom $H(x)$ and a single scalar particle, the Higgs Particle. [5] The scalar Lagrangian now describes three massive bosons, $W^\pm$ and Z. It takes the form:

$$\mathcal{L}_\phi = \left(1 + \frac{H}{v}\right)^2 \left\{ M_W^2 W_\mu^\dagger W^\mu + \frac{1}{2} M_Z^2 Z_\mu Z^\mu \right\} + \mathcal{L}_H \tag{2.5}$$

with the Higgs Lagrangian:

$$\mathcal{L}_H = \frac{1}{2}\partial_\mu H \partial^\mu H - \frac{1}{2} M_H^2 H^2 - \frac{M_H^2}{2v} H^3 - \frac{M_H^2}{8v^2} H^4 \tag{2.6}$$

For boson masses we receive:

$$M_W = M_Z \cos\theta_W = \frac{1}{2}gv \tag{2.7}$$

The weak mixing angle defines the Z and γ fields:

$$\begin{pmatrix} W_\mu^3 \\ B_\mu \end{pmatrix} = \begin{pmatrix} \cos\theta_W & \sin\theta_W \\ -\sin\theta_W & \cos\theta_W \end{pmatrix} \begin{pmatrix} Z_\mu \\ A_\mu \end{pmatrix} \tag{2.8}$$

and is related to the gauge couplings through $g\sin\theta_W = g'\cos\theta_W = e$. The afford mentioned measured boson masses imply $\sin^2\theta_W = 1 - M_W^2/M_Z^2 = 0.223$. [8] For the next step, we need to add the relationship between $W_\mu^{1,2}$ and the weak bosons $W^\pm$:

$$W_\mu^\pm = \frac{1}{\sqrt{2}}(W_\mu^1 \mp iW_\mu^2) \tag{2.9}$$

After inserting this and 2.8 into the gauge equations we get the quark hypercharge assignments and the $W^\pm$ and Z mass terms.

$$M_W = \frac{g_W v}{2} \qquad M_Z = \left(\frac{g_W v}{2}\right)\left(\frac{g_y}{g_W}\sin\theta_W + \cos\theta_W\right) = \frac{g_W v}{2cos\theta_W} \tag{2.10}$$

Resulting in a value for $v = 246$ GeV. With the experimentally obtained Higgs mass, a parameter of the SM, the quartic scalar coupling, $\lambda = \frac{M_H^2}{2v^2} = 0.13$ can be determined. [4, 5]

2.3 Polarisation

Polarisation is the product of the particle's spin vector and the direction of the momentum vector. We already established that longitudinal polarisation is necessary for the boson mass generated by the EWSB. Vector boson-polarisation is therefore connected to one of the innermost SM mechanisms that are the subject of current research. We describe the polarisation with the helicity operator:

$$h = \frac{\vec{p}\cdot S}{|\vec{p}|} \tag{2.11}$$

$W^\pm$ and Z bosons are spin-1-particles, their possible eigenvalues of h are $-1, 0$ and $+1$. For eigenvalues ± 1 the spin is parallel or antiparallel to the momentum, for 0 it is orthogonal to the momentum of the particle. Since the helicity depends on the momentum it is only Lorentz invariant for massless particles, since faster Lorentz-boosts can always flip the direction of helicity while boosting massless particles into a faster reference frame is not possible and therefore their helicity is Lorentz invariant.[9, 10]

The first step to describe polarisation is by combining the free field theory:

$$\mathcal{L} = -\frac{1}{2} F^{\dagger}_{W\alpha\beta}(x) F^{W\alpha\beta}(x) + m_W^2 W^{\dagger}_{\alpha}(x) W^{\alpha}(x) \tag{2.12}$$

and the Lagrangian for spin-1 particles, the Proca Lagrangian with $\partial_\mu W^\mu = 0$. Using the Euler-Lagrange Equations, equations of motion can be derived from 2.12.

$$\Box W^{\alpha}(x) + m_W^2 W^{\alpha}(x) = 0 \tag{2.13}$$

This results in the solution:

$$W^{\alpha(x)} = \int \frac{d^3q}{(2\pi)^3 2q_0} \sum_{\lambda} \epsilon^{\alpha}(q,\lambda)\hat{a}(q.\lambda)e^{-iqx} + \epsilon^{*\alpha}(q,\lambda)\hat{b}^{\dagger}(q,\lambda)e^{iqx} \tag{2.14}$$

The definition of polarisation is not fixed, there are two different choices to make. First, a spin axis has to be chosen. Usually, this is the helicity base. The polarisation vectors become the eigenvectors of the helicity. As already established, the helicity is not Lorentz-invariant, therefore it is also necessary to choose a frame to define the polarisation vectors. Two possibilities are investigated: the Laboratory frame of the detector(LAB) and the centre-of-mass frame (CM). The polarisation vectors:

$$\epsilon^{\mu}_{\pm}(\mathbf{p}) = \frac{e^{\mp i\phi}}{\sqrt{2}}(0, -\cos\theta\cos\phi \pm i\sin\phi, -\cos\theta\sin\phi \mp i\cos\phi, \sin\theta) \tag{2.15}$$

$$\epsilon^{\mu}_{0}(k) = s^{\mu}_{k} = \frac{k^0}{m}\left(\frac{|k|}{k^0}, \cos\phi\sin\theta, \sin\phi\sin\theta, \cos\theta\right) \tag{2.16}$$

with k^μ being the vector-boson momentum.

To observe the polarisation modes of weak bosons we have to study their decay products since the bosons themselves are off-shell and unstable. They have to be reconstructed out of the hadrons and leptons they produce. Special attention is to be paid to the angular variables which are directly dependent on the polarisation mode. [11]

Propagators that describe virtual vector bosons do not include polarisation vectors:

$$\frac{i\left(-g_{\mu\nu} + \frac{q_\mu q_\nu}{m_V^2}\right)}{q^2 - m_V^2 + i\Gamma_V m_V} \tag{2.17}$$

By substituting Dirac spinors in the completeness relation with polarisation vectors propagators can be dependent on polarisation.

$$\sum_{\lambda} \epsilon_{\lambda}^{*\mu} \epsilon_{\lambda}^{\nu} = -g^{\mu\nu} + \frac{q^{\mu} q^{\nu}}{m^2} \tag{2.18}$$

This is part of the propagator, which includes polarisation vectors. [4]

Concluding the last two chapters, polarisation is directly tied to EWSB and therefore a parameter that has the potential to probe SM gauge symmetry structure and Higgs-Mechanism. Any deviation from SM predictions about the production of longitudinally polarised electroweak boson could lead to Beyond Standard Model (BSM) physics.

2.4 LHC and Proton-Proton Collisions

The Large Hadron Collider(LHC) is a 27 km long particle accelerator ring that is the latest addition to the Conseil Européen pour la Recherche Nucléaire complex (CERN), which belongs to the CERN organisation, an intergovernmental organisation operating the largest particle physics laboratories in the world. The CERN complex is located underground spanning over the swiss-french border near Geneva. The LHC itself conducts proton-proton collisions by forcing two proton beams into each other, focused and kept on track through a variety of superconducting magnets cooled by liquid helium, sped up by a number of smaller preceding accelerators. On the LHC itself, eight experiments are conducted, with four of them being the particle detectors ATLAS, ALICE, CMS and LHCb. The biggest achievement of this collider and the participating experiments was the discovery of the Higgs boson in 2012.
The conducted proton-proton collisions will collide at a centre of mass (LAB) energy between $\sqrt{s} = 2.36\ TeV$ and $\sqrt{s} = 13.6\ TeV$ depending on the run of LHC. [12] These proton-proton collisions are strongly inelastic interactions with momentum transfers corresponding to the order of magnitude of the LAB energy, emitting so-called particle jets that are caught in the surrounding detectors. The jets are products of the interactions between the fundamental particles, largely gluons, quarks, and anti-quarks since these are the particles protons contain. These processes are divided into two categories, hard and soft scattering. The base of all processes is QCD, but different levels of understanding is required for the cases. Hard processes merely require perturbation theory to achieve good precision, different to the rates and production of soft processes that they need non-perturbation QCD-effects, which are less well understood. [13]

2.4.1 Scattering Parameters

Scattering parameters are the data that are output by scattering experiments. By using the different detectors implemented in e.g. ATLAS, one can extract four-momentum vectors of the decay products that reach the detector after processes took place in the collision point or in close vicinity. Four momentum vectors are traced back to find out the process position and other incoming particles originating in the same process.
The components of the four-momentum vector are the first parameters that are used to study processes. They contain the particle energy **E** and the three-dimensional momentum **p**. This also gives us the invariant mass **m**. Using the four-vectors of the decay products we can also draw conclusions about the initial and intermediate particles. Using the detectors that the particle interacted with and its invariant mass, we know the species of the particle and can thereby narrow the possible intermediate and initial particles down. The frame the collisions take place in is oriented to have the initial particle beams on its z-axis, resulting in initial momenta $p_{x,i} = p_{y,i} = 0$. The momentum vector in the plane orthogonal to the beam axis is called transverse momentum $\vec{p_T} = (p_x, p_y)$. Decay angles, e.g. in reference to the beam axis, are the polar angle θ and azimuthal angle ϕ. A two-dimensional version of scattering in a Laboratory frame (LAB frame) can be seen in figure 2.2. It will be useful to boost the frame so a particle only moves perpendicular to the beam axis since the kinematics of decay become simplified for this case. When doing this two new parameters come into play, rapidity and pseudorapidity. Rapidity differences Δy are Lorentz invariant for boosts along the z-axis and therefore a useful tool to describe particles in the LAB frame of the particle beams.

$$y = \frac{1}{2} \ln \left(\frac{E + p_z}{E - p_z} \right) \tag{2.19}$$

The pseudorapidity η is an approximation for high-energy beams when masses are comparatively small.

$$\eta = -\ln \left(\tan \frac{\theta}{2} \right) \tag{2.20}$$

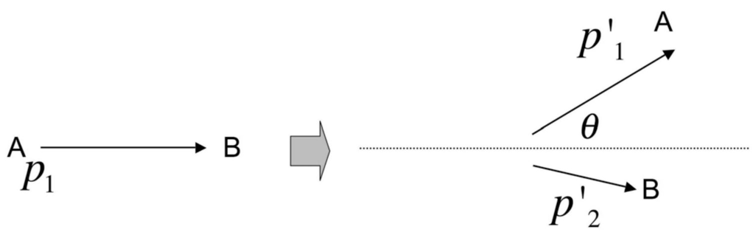

Figure 2.2: Elastic scattering in a LAB frame[5]

Boosting a decay product in the rest frame of their initial particle can also be useful. For example, consider the W^+-boson. Its momentum will be mostly aligned along the beam axis, while the positron will have a large transverse momentum. This results in a large angle between the W^+ momentum and the positron. The p_{T,e^+} is closely tied to the decay angle θ^* in reference to the original W^+ motion vector when boosting the positron into the rest frame of the W^+ boson. While doing this, the transverse momentum stays the same. This process is shown in figure 2.3.[5]

$$p_T = |\vec{p_{e^+}}| \sin\theta^* \cong E_{e^+} \sin\theta^* = \frac{M_W}{2} \sin\theta^* \tag{2.21}$$

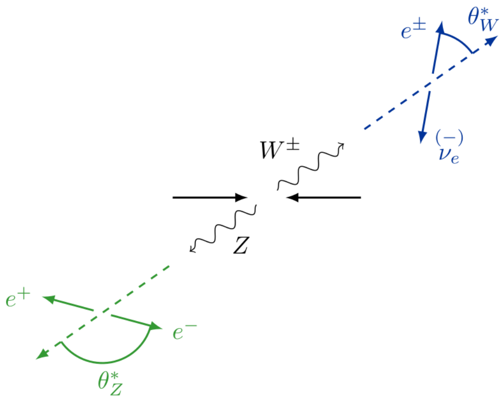

Figure 2.3: θ^*_X Definition, black LAB frame, blue $W^{\pm}$ rest frame, green Z rest frame [14]

2.5 W^+Z Production

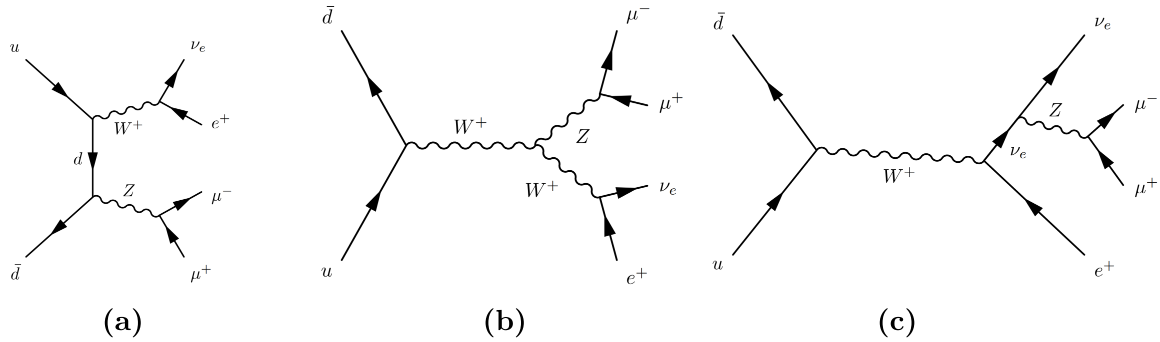

Figure 2.4: W^+Z Production, resonant(a,b) and non-resonant (c) example (for all possible processes, see appendix A.4)

Examples of the processes that are used to validate the Sherpa implementation can be seen in figure 2.4. Generally, processes that have a quark and an antiquark as an initial particle and one muon, one antimuon, one electron neutrino and one electron as final products are investigated. Four electroweak interactions are allowed. This does result in a leading order process with at least one W boson. It is possible to substitute the Z with a photon. In this thesis, only W^+Z production will be investigated. W^-Z production will receive no explicit analyses, but all analyses and simulations are entirely analogue and the run cards are easily adaptable. The decay angle that has been already discussed can be used to create matrix elements that can predict the differential cross section(dXS) in reference to $\cos\theta^*_X$, resulting in two equations:

$$\begin{aligned}\frac{1}{\sigma}\frac{d\sigma}{d\cos\theta^*_Z} = \frac{3}{8}&\left(1+\cos^2\theta^*_Z - \frac{2(c_L^2-c_R^2)}{c_L^2+c_R^2}\cos\theta^*_Z\right) f_{-1}\\ +\frac{3}{8}&\left(1+\cos^2\theta^*_Z + \frac{2(c_L^2-c_R^2)}{c_L^2+c_R^2}\cos\theta^*_Z\right) f_{+1}\\ &+\frac{3}{4}\sin^2\theta^*_Z f_0\end{aligned} \tag{2.22}$$

$$\frac{1}{\sigma}\frac{d\sigma}{d\cos\theta^*_W} = \frac{3}{8}(1-\cos\theta^*_W)^2 f_{-1} + \frac{3}{8}(1+\cos\theta^*_W)^2 f_{+1} + \frac{3}{4}\sin^2\theta^*_W f_0 \tag{2.23}$$

By isolating the polarisation modes f_{-1}, f_{+1} and f_0 we can predict their dXS with respect to the decay angle. The results are shown in figure 2.5.[14]. When measuring specific processes there

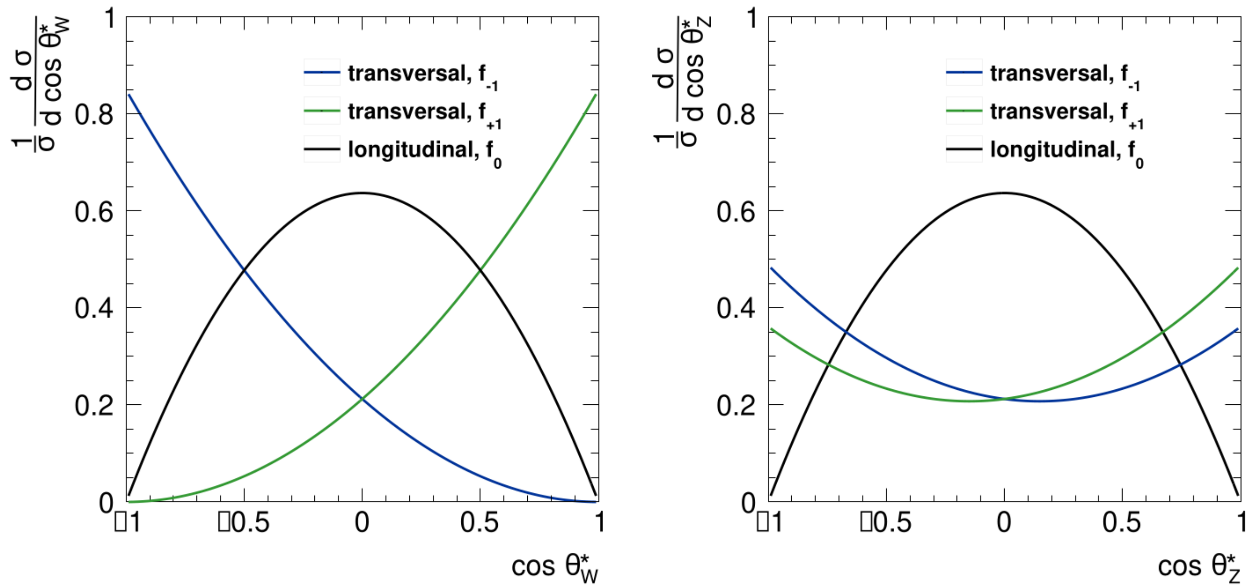

Figure 2.5: Normalized differential distribution of the XS over $\cos\theta_{W/Z}$[14]

is always a so-called non-resonant background, due to processes that do not meet the energy requirements to interact via the particles of interest. Figure 2.4c is an example for the process of this thesis that does not meet the energy conditions. For them, no polarisation definition is possible. Due to gauge invariance, they cannot be simply ignored and approximations need to be applied, which are discussed in section 3.2. Both resonant and non-resonant processes

are part of the $W^{\pm}Z$ production. Additionally, there are contributions from processes that involve photons that can be suppressed by cuts.
Interferences are a byproduct of squaring the matrix element when the completeness relation is used to add polarised vector bosons. We will use a relatively simple example to show the appearance of interferences, single W production and decay with matrix elements for production $\mathcal{M}_\lambda^{\mathcal{P}} = \mathcal{M}_\lambda{}^{prod}\epsilon_\lambda^{*\mu}$ and decay $\mathcal{M}_\lambda^{\mathcal{P}} = \mathcal{M}_\lambda{}^{decay}\epsilon_\lambda^{*\mu}$.

$$\begin{aligned}\mathcal{M} &= \mathcal{M}_\mu^{prod}\frac{i\left((g^{\mu\nu} + \frac{q^\mu q^\nu}{m_W^2}\right)}{q^2 - m_W^2 + i\Gamma_W m_W}\mathcal{M}_\nu^{decay} \\ &= \mathcal{M}_\mu^{prod}\frac{i\sum_\lambda \epsilon_\lambda^{*\mu}\epsilon_\lambda^{\mu}}{q^2 - m_W^2 + i\Gamma_W m_W}\mathcal{M}_\nu^{decay} = \frac{i}{q^2 - m_W^2 + i\Gamma_W m_W}\sum_\lambda \mathcal{M}_\lambda^{\mathcal{P}}\mathcal{M}_\lambda^{\mathcal{D}} := \sum_\lambda \mathcal{M}_\lambda^{\mathcal{F}}\end{aligned} \tag{2.24}$$

$$\sigma \propto |\mathcal{M}| = \sum_\lambda |\mathcal{M}_\lambda^{\mathcal{F}}|^2 + \sum_{\lambda,\lambda'} \mathcal{M}_\lambda^{\mathcal{F}} * \mathcal{M}_{\lambda'}^{\mathcal{F}} \tag{2.25}$$

The last term of equation 2.25 is the interference term, where the matrix elements of different polarisation modes are used. The first term is proportional to the polarised XS for a helicity λ. Since interferences are disturbing factors these have to be considered in the analysis to minimize their effects. For the rare case that no lepton cuts are applied, the sum over all interferences does equal zero. [9, 11]

3 Simulation and Analysis Framework

3.1 Monte Carlo Event Generators

In high-energy particle physics, event generators are used to interpret data from colliders, in order to measure fundamental physics parameters and to test for new physics. [15]Physicists have developed a wide range of tools to predict the results of colliders, including scattering cross sections, differential distributions and event topologies [16].
Over the past years, the current knowledge has been implemented using numerical Monte-Carlo techniques, the event generators their name. QED is implemented, playing a crucial role in the simulation of collision and scattering events, delivering these simulations in an exceptionally precise manner. [15, 16]
The event generator used for this work, Sherpa, short for Simulation of High-Eenergy Reactions of Particles, is able to simulate all possible collision combinations between leptons, hadrons and photons. We are using LHC beam data, so naturally, we only deal with proton-proton collisions. It is configured via a text file, the run card, that specifies the simulation settings and the process definition. After that, two built-in tree-level generators named AMEGIC and COMIX are able to simulate parton-level events with the laws of the SM and BSM if required. They can simulate decays of heavy resonances found in W, Z or Higgs-bosons and top quarks, the latter is crucial to our interests in this thesis. It is also worth mentioning that, since most of the time one is interested in events from specific processes, the simulation is built around a hard subprocess rather than simulating typical events and waiting for the desired, but sometimes very rare events.[17]
The hard collisions that were investigated start at the parton-level. The event generation starts there and begins with simulating interactions between the predefined fundamental particles, distributing hard parton momenta by using their corresponding QFT transition matrix element.[15] Hard partons are simplified to individual observable jets, making the evaluation of production rates and differential distributions of complex multijet final states with realistic detector acceptances possible. Additionally, the implemented showering and hadronization algorithms are the starting point to describe the final state and make event generators the foundation of most analyses.
Differential cross sections for general hadron-hadron collisions are calculated with f_i, parton

distribution functions (PDF), and the corresponding matrix elements $|M|^2$:

$$\frac{d\sigma}{d\Omega dx_1 dx_2} = \frac{1}{Flux} \sum_{i,j,k,...n} f_i(x_1, \mu_F) f_i(x_2, \mu_F) \times \bar{\sum} |M(i,j \to k,l,...n)|^2 \tag{3.1}$$

The PDF is made up of the parton i and its momentum fraction x_1 probed in the proton at a scale of μ_F. This is then summed up other the partons contained by the proton, while the second sum adds up the averages of the squared matrix elements. This is all done by the parton-level event generator. [15] Since the collision of particles is a rather complicated process the Monte Carlo methods used to imitate them are equally complicated and broad. We will only take a brief look at the basics of Monte Carlo numerics, more detailed explanations are in the linked sources [17].

Cross sections are a measure of probability, so naturally, we are interested in distributions of cross sections over different suitable parameters. The processes we analyze are mainly defined by their location in phase space, in which the probability distribution is realized by the abundance of points in certain areas and locations. The most simple case is a phase space that consists of one variable x. Provided the probability density distribution of x is proportional to $f(x) \geq 0$, x can be generated by using the integrals:

$$\int_{x_{\min}}^{x} f(x')dx' = R \int_{x_{\min}}^{x_{\max}} f(x')dx' \tag{3.2}$$

under the conditions that x is part of $[x_{min}, x_{max}]$ and $R \in [0,1]$ is a uniform pseudo-random number. This problem becomes trivial when the inverse function of f, F^{-1}, is known. Equation 3.2 is in this case equivalent to $F(x) = RF(x_{max}) + (1-R)F(x_{min})$. For unknown inverse functions, the solution can be found numerically thanks to the monotony of $F(x)$ due to $f(x) \geq 0$. However, if $F(x)$ is unknown or too computationally expensive a function with a known indefinite integral $G(x)$ of $g(x)$ can be used, under the condition that $g(x) \geq f(x)$ on the x-interval. For this method to work $G(x)$ has to be solvable or invertible for x. The generated distribution by exchanging $g(x)$ for $f(x)$ is then accepted with probability $f(x)/g(x)$ for the resulting points. By choosing a constant $g(x) = g_u \geq \max f(x), x \in [x_{min}, x_{max}]$, uniform points are generated by

$$x = Rx_{max} + (1-R)x_{min}, \tag{3.3}$$

which are accepted if $f(x) > R'g_u$ is valid, with $R' \in [0,1]$ being another uniform pseudo random number. This method can be relatively inefficient provided that g_u is too large or $f(x)$ not being uniform enough, resulting in its name hit-or-miss method.

When considering a phase space that has more than one variable, so for example in our case, $f(\vec{x})$ is a matrix element squared as a function of a n-component vector $\vec{x}$ and is integrated over a region V of $\vec{x}$-space:

$$I[f] = \int_V d^n x f(\vec{x}) \tag{3.4}$$

At this point, the default methods of integration become too computationally expensive and/or inaccurate due to the number of dimensions. We can go around this problem by pseudo-randomly scattering N points in V, and then the mean value of f can be approximated:

$$I[f] \simeq \langle f \rangle = \frac{1}{N} \sum_{i=1}^{N} f(\vec{x}_i). \tag{3.5}$$

The variance of f gives provides an error $E[f]$ for this approximation.

$$Var(f) = \langle f^2 \rangle - \langle f \rangle^2 \tag{3.6}$$

$$E[f] = \sqrt{\frac{\mathrm{Var}(f)}{N-1}} \tag{3.7}$$

The error is inversely proportional to the square root number of points. There are further methods to reduce the error, e.g. importance sampling and methods when singularities in $f(x)$ occur, mainly for NLO cross sections. When hit-or-miss will fail to converge, the variance will diverge and variance reduction becomes necessary. These and many more methods belong to the MC numeric tool kit and are necessary to simulate events of complex particle collisions. [17]

3.2 Polarisation in Event Generators

Polarisation of bosons is implemented in a few event generators, e.g. Madgraph[18], Phantom[19] and Whizard [20]. To simulate polarisation, one first needs to take a look at the processes that are involved.

The process in figure 2.4c represents a range of processes that are not doubly-resonant and can not be interpreted as vector boson pair production. They cause an irreducible background that can and should not be neglected. Non-doubly-resonant processes are, on the other hand, necessary to preserve the gauge invariance, which means we cannot subtract them without having a way to compensate for this background. [11]

3.2.1 Narrow Width Approximation

One way and the way that is used in the Sherpa implementation, to compensate for this is the narrow width approximation (NWA). There are five conditions that are required to use NWA:

1. $\Gamma << M$, the width Γ being smaller when the mass M of the resonant particle
2. $m << M$, m representing the mass decay products
3. $\sqrt{s} >> M$, $\sqrt{s}$ being the scattering energy
4. no significant resonances with non-resonant processes
5. the resonant propagator is separable from the matrix element

[21] In our process, all these requirements are met. [9]. Note that point two is especially beneficial for EW-boson decay. Therefore we can make the approximation:

$$\frac{1}{(q^2 - m_W^2)^2 + \Gamma_W^2 m_W^2} \rightarrow \frac{\pi\delta(q^2 - m_W^2)}{\Gamma_W^2 m_W^2} \tag{3.8}$$

NWA replaces Breit-Wigner distribution by assuming that the massive state is always exactly at its pole, representing an asymptotic final state. This dramatically simplifies the decaying process which is now expressed by a fractional probability to decay into a specific final state, the branching ratio(BR). NWA provides an error $\mathcal{O}(\Gamma/M)$, causing a preferred use for NWA when Γ/M is relatively small.[21]
It is crucial to mention that NWA tends to be very inaccurate under certain circumstances. The causes are the neglect of off-shell effects and spin correlations. [11]
To counter the latter, the Sherpa implementation uses a spin-correlation algorithm. [22] After the calculation of the production element, a random outgoing particle is chosen and its spin density matrix is calculated. After one decay, channels are chosen in correspondence with their branching ratios. With the decay channel chosen, the momenta of the decay products can be calculated and therefore the decay matrix is clear if all decay products are stable. Off-shell effects are recovered by performing a mass smearing of the intermediate particles according to the Breit-Wigner distribution.[9]

3.2.2 Double Pole Approximation

Double-Pole Approximation(DPA) is a proven alternative to NWA. In contrast to NWA, DPA leaves the Breit-Wigner off-shell, while the numerator of the resonant processes will be projected on-shell to preserve gauge invariance, given a resonant amplitude. This separates the irreducible background and the resonant boson pair production while retaining gauge invariance. [11]

3.3 Data Analysis with Rivet

The final purpose of data that is produced with MC-event generators and detectors is to be compared with its theoretical/experimental counterpart. To make this data comparable we have numerous tools and we will be using Rivet. It provides a collection of experimental analyses and their underlying infrastructure. Rivet has a C++-based object-oriented framework. None of the countless available analyses fits our needs, so we will develop our own.[23] Sherpa can output event files containing generated events according to a run card. These files can be analysed separately by Rivet.

Concluding from this and the previous chapters it is only natural to include polarised cross sections into the Sherpa framework, which is not the case in the newest stable version. This is currently being implemented by Mareen Hoppe at the Institut for Nuclear and Particle Physics at Technical University Dresden [24]. Hoppe has already been successful in testing the implementation for W^+W^+jj and W^+j production.[9] Testing this modification of Sherpa for $W^\pm Z$ production is a logical next step. To verify the results we compare with [25] to calculate the cross sections of polarised cross sections we calculated at LO and NLO by using the double-pole approximation and the separation of polarisations at the amplitude level. [25]

4 Simulation, Analysis and Results

4.1 Simulation Configuration

We will be using the Sherpa installation Sherpa version 3.0.0 with the implemented polarisation calculation on the ZIH High-Performance Computing (HPC) Grid of the TU Dresden. For the analyses, the cuts that have been implemented are taken from the paper "NLO QCD predictions for doubly-polarised WZ production at the LHC"[25]. The phase space selected through cuts in the paper and in the simulation is based on the cuts that are applied during the corresponding experimental analysis with the ATLAS detector[26]. This leads to a fiducial signal region that resembles the detector's signal region. In addition, the beam parameters of run 2 at the LHC are used to provide distributions that can be compared to experimental results if necessary.
Simulating polarised cross sections requires settings that do not allow processes without a polarsation definition. Therefore, two separate simulations need to be conducted: one for the full cross sections, with all possible processes, and one for the polarised cross sections. Two simulations need two run cards, which can be seen in appendix A.1 and A.2. The full calculation includes inclusive non-resonant contributions and off-shell effects. The polarisation run card enables the spin-correlated NWA and Mass-Smearing. Concluding this, the Sherpa configuration chooses the following settings:

- **Set up**: LHC Beam Data, so proton-proton collisions with 6500 GeV per beam
- **Hard process**: $jj \to e^+\nu_e\mu^-\mu^+$, fixed order: EW:2, QCD:0
- **Factorization/Renormalization scale**:

  $$\mu = \frac{M_W + M_Z}{2}$$

- **Inclusive cuts during the simulation**:
  - interval for invariant muon-antimuon-pair mass: $81\,\text{GeV} \leq m_{\mu^+,\mu^-} \leq 101\,\text{GeV}$
  - minimum for transversal positron momentum: $p_{T,e^+} > 20\,\text{GeV}$
  - minimum for transversal (anti)muon momentum:$p_{T,\mu^\pm} > 15\,\text{GeV}$
  - maximum absolute rapidity cut for all charged leptons: $|y_{e^+,\mu^\pm}| < 2.5$

  - minimum rapidity-azimuthal-angle distance cut for lepton pairs: $\Delta R_{\mu^+\mu^-} > 0.2$ and $\Delta R_{\mu^\pm e^+} > 0.3$
  - minimum cut on the W-boson transverse mass $M_{T,W} > 30$ GeV

- **PDF-Set**: NNPDF31_lo_as_0118

- **EW-paramter**:
  - EW-scheme: G_μ
  - $G_F = 1.16638 \times 10^{-5}\,\mathrm{GeV}^2$
  - $M_W = 80.351971594\,\mathrm{GeV}$
  - $M_Z = 91.153480619\,\mathrm{GeV}$
  - $\Gamma_W = 2.084298894\,\mathrm{GeV}$
  - $\Gamma_Z = 2.494266379\,\mathrm{GeV}$

The Sherpa run card can be found in appendix A.1.
The EW-scheme sets the parameters of the SM that are considered fixed and the parameter that are determined by the given quantities. In the used scheme the Fermi constant, $W^\pm$, Z, and Higgs masses and widths are fixed. Since there is no clear way of determining α_{EW} a convention has to be chosen. The convention used fixes the weak mixing angle with $c_W = M_W/M_Z, s_W^2 = 1 - c_W^2$. α is exchanged for G_μ to use effective coupling:[27]

$$\alpha_{G_\mu} = \frac{\sqrt{2} G_\mu M_W^2 s_W^2}{\pi} \tag{4.1}$$

The rapidity-azimuthal-angle is calculated by using the pseudorapidity distance $\Delta\eta$ and the azimuthal angle difference $\Delta\phi$:

$$\Delta R = \sqrt{(\Delta\eta)^2 + (\Delta\phi)^2} \tag{4.2}$$

The W-boson transverse mass is determined by using the transverse momenta of its decay leptons $p_{T,e^+} p_{T,\nu_e}$ and the azimuthal angle difference between them $\Delta\phi_{e^+\nu_e}$.

$$M_{T,W} = \sqrt{2 p_{T,\nu_e} p_{T,e^+} (1 - \cos\Delta\phi_{e^+\nu_e})} \tag{4.3}$$

For the properties of the bosons, the pole variants will be used. The pole mass is the pole of the particle propagator and is close to what could be phrased as an observable particle mass. It can also be seen as the limit of the rest mass at high energies. They are calculated by using the on-shell masses and width:

$$M_W^{OS} = 80.379\,\mathrm{GeV}, \quad \Gamma_W^{OS} = 2.085\,\mathrm{GeV} \quad M_Z^{OS} = 91.1876\,\mathrm{GeV} \quad \Gamma_Z^{OS} = 2.4952\,\mathrm{GeV}$$

The pole values are then obtained by the means of [11]:

$$M_V = \frac{M_V^{OS}}{\sqrt{1 + (\Gamma_V^{OS}/M_V^{OS})^2}} \qquad \Gamma_V = \frac{\Gamma_V^{OS}}{\sqrt{1 + (\Gamma_V^{OS}/M_V^{OS})^2}} \tag{4.4}$$

The implementation of polarised cross sections allows choosing the spin basis as the helicity basis and the reference frames, vector boson Centre of Mass and Laboratory frame. When applying NWA, the matrix elements can be separated in production and decay. This is mirrored by Sherpa by specifying the intermediate particles in a hard process $q\bar{q} \to W^+Z$ and forcing the decay of both bosons into the needed products. Therefore, non of the lepton cuts can be applied during this simulation. The remaining simulation parameters remain unchanged, excluding the widths of the bosons, which have to be set to zero for the hard process. Also, the HARD_DECAY parameters had to be added, setting Mass_Smearing to 1 and consequently exchanging a fixed mass of the vector bosons for a probability distribution, in this case, a Breit-Wigner shape. This affects only the kinematics, the matrix elements remain calculated by the NWA. [27]

4.2 Rivet Analysis

Rivet will provide us with the appropriate tools to plot the distributions we need and also calculate the distributions that were used in the DPA simulation. The Rivet analysis written for this simulation can be seen in appendix A.3. From lines 2 to 8 the needed classes, so pre-build tools that Rivet provides, are imported. Lines 12 to 36 include a class that will be needed for the determination of the neutrino momentum and the finding of W^+-bosons, therefore providing multiple helpful attributes including objects of the class particle to represent the decay products. After that, the analysis class MC_WZ_polar is established. Rivet analysis classes consist of three main methods: init()[l.50-l.81], analyze()[l.109-l.174] and finalize()[l.177-l.189]. The init() creates the necessary structures to find the particles we are looking for in the event files and books the histograms we intend to display. The analyze() conducts all kind of filtering and finding of events, it is here the function finds the events that contain the wanted processes and apply the lepton cuts of the simulation again. This is necessary since the polarised cross section simulation cannot apply these cuts. Additionally, by adding prints, the simulation of the full cross section can be tested. In the last part of the analyze() function, we fill the histograms with the events that weren't cut out. Finally, the finalize() provides the option to scale the histograms, which is done by dividing through the cross section, the unit of the cross section and the weighted sum of events. After that the nature of a histogram is provided, we exclusively use 1D in the private section of the analysis class.

The parameter mentioned in the first sentence is the decay angle between the lepton and boson in the rest frame of the boson. To determine this parameter two functions, one for each definition of polarisation, have been added in lines 84 to 104. These functions boost the lepton into the restframe of the boson and the transformed momentum vector into a system where the boson momentum is aligned to the z-axis. In the case of LAB frame, the boson first has to be transformed into the LAB frame of both bosons, before undergoing the same procedure as the LAB frame function.

One problem of analyses of processes that involve neutrinos, especially when the goal is to compare them to experimental data, is neutrino reconstruction. Neutrinos rarely interact with any detector, so the data we get from other, detected particles, has to be used to reconstruct them out of the energy that is missing in certain processes and assigned to neutrinos. The comparison paper [25] assumes perfect neutrino construction. Since no further details are given, the reconstruction in our simulation will happen by using the IdentifiedFinalState class that returns neutrinos with clear properties and data as if it was possible to detect all of them. The same is done to find the corresponding positron and their four-momentum vectors are used to construct the W^+-boson. Multiple reconstruction methods have been tested, including the WFinder class and calculating the missing neutrino momentum along the beam axis.[26] Taking the neutrino directly out of the FinalState is most true to the wording of the paper and results in the best cross sections and graphs, therefore this will be the used method.

4.3 Study of Generated Events

With the analysis and the Sherpa run cards set, the events can be generated and analysed to create the histograms and cross sections. The results will be put into direct comparison with the cross sections and histograms of the DPA[25]. These histograms display the NLO parameters in their main plot and include a NLO/LO ratio plot lowest the main differential cross section over the parameter plot. Since the simulation conducted in this thesis only includes LO, when looking at the values and in some cases the shape, the ratio plot will as important as the main plot to compare the results. To reduce statistical errors the number of generated events has been set to five million for the full-, and 20 million for the polarised Sherpa run. Since the cuts of the polarised Sherpa run can only be applied after the generation, the number had to be considerably higher. In this chapter, the terms LAB frame and CM frame always refer to the polarisation corresponding polarisation definition when not specified otherwise. Acronyms will also be used for the polarisation modes, replacing $W^+_{L/T}$ with L/T as the first letter and $Z_{L/T}$ with L/T as the second letter. For example, $W_L Z_T$ will be LT.

4.3.1 Integrated Cross Sections

Table 4.1 shows all relevant cross sections, fractions and uncertainties. The fraction uncertainties were insignificant, ranging between 10^{-4} and 10^{-5}. The XS uncertainties are the rivet

	$\sigma_{NWA}[fb]$	$\sigma_{DPA}[fb]$	$fraction_{NWA}$	$fraction_{DPA}$
full	19.547(12)	19.537(7)	-	-
unpolarized	18.402(20)	19.125(6)	1.000	1.000
Cross-Sections with Polarisation Definition in the Lab Frame				
$W_T Z_T$	9.967(10)	10.526(4)	0.542	0.550
$W_T Z_L$	4.223(9)	4.381(2)	0.229	0.229
$W_L Z_L$	1.044(2)	1.0824(4)	0.057	0.057
$W_L Z_T$	3.064(7)	3.165(1)	0.167	0.165
Cross-Sections with Polarisation Definition in the CM Frame				
$W_T Z_T$	12.788(20)	13.555(5)	0.695	0.714
$W_T Z_L$	1.799(3)	1.902(1)	0.098	0.100
$W_L Z_L$	1.457(2)	1.508(1)	0.079	0.079
$W_L Z_T$	1.950(4)	2.018(1)	0.106	0.106

Table 4.1: Integrated cross section for a fiducial setup including unpolarised, full and doubly polarised. Both polarization definitions, CM and LAB frame, are taken into account. Fraction represent the ratios of polarised over the unpolarised cross-section

integration errors.

The full cross sections of DPA and NWA agree since they lie in the margin of error. Full XS integrations do not include DPA or NWA, this confirms an agreement of the event generators and analyses. The Rivet analysis is thereby valid and a comparison of the polarised XS obtained with Sherpa to the DPA XS is justified. Additionally, the full XS includes all resonant and non-resonant processes, making it an important reference.

As a general phenomenon, frame independent, the TT polarisation has by far the highest and the LL has always the lowest XS, indicating a heavy favouring of transversal polarised bosons. While the mixed polarisations possess the second and third highest XS, it depends on the rest frame which one will end up in which position. This is true for both NWA and DPA.

By comparing the polarised XS of NWA and DPA we see that there is a significant difference of 5.5%(CM) to 6%(LAB). The NWA has lower XS, which points to a systematical cause. A likely cause is the approximations, especially since similar behaviour has been observed for different processes. Despite the unpolarised cross sections not being influenced by the polarisation implementation, it has the same negative deviation when compared to its DPA counterpart, implying a working polarisation implementation. However, when looking at the fractions we see a satisfying compliance that does support a cause founded in the approximation rather than the polarisation implementation.

When comparing the mixed polarisation modes, the LAB frame is closer than their LAB frame counterparts. This is likely due to the momentum of bosons in the CM frame being exact opposites of each other, having only their sign as a difference. The remaining deviation between them could be explained by the W^+ bosons not interacting with right-handed fermions.

Another interesting take is the influence interferences have on the polarised modes. The caused effects reach about 2.3% for the CM and 0.6% for the LAB frame. Lepton cuts cause non-vanishing interferences and are a likely cause for these deviances from the unpolarised result.

4.3.2 Distributions

In figures 4.1 to 4.5 differential distributions are shown for multiple important kinematic variables, which were discussed in Section 2.4.1. Plots that are located on the left side of their page are plots generated and analysed with Sherpa and NWA, while right-side plots were generated in the paper [25] with PHANTOM and DPA. These plots depict showing a normalized shape below their main plot. The NWA plots on the other display the LO in their main plot with two ratio plots below that, one on a large range on the z-axis to show every polarised mode and one with a small interval, to make it possible to deviate the sum of polarisations and the unpolarised dXS. Each figure contains four distributions, the lower ones use the polarisation definition in the LAB frame, while the other two are generated with the CM frame definition.

Figure 4.1 considers the positron decay angle in the W^+-boson rest frame. In general, the difference between the unpolarised dXS and the full dXS can be considered as the non-resonant background. Interference between polarised modes can be taken from the difference between the sumpol and the unpolarised dXS. This difference largely remains below 4% of the full dXS in all kinematic variables except for the rapidity. It is noticeable that interference in CM frames is higher than in LAB frames and that the DPA approximation generally has a lower non-resonant background, likely due to the already mentioned differences between DPA and NWA.

When comparing both approximations the shapes resemble each other. There may be some regions where the curve does have different rates of change, but when taking the NLO/LO DPA ratio plot into account it is safe to say that the DPA results could be reproduced similar to the integrated cross sections.

The fall off of both approximations for $\cos\theta_{e^+}$ near -1 can be attributed to the cuts imposed on the lepton. Would cuts be applied to the neutrino, a sharp decline could be observed at $\cos\theta_{e^+} \rightarrow 1$, since the transverse momentum becomes small for the neutrino there.

The asymmetric shape of all distributions that do involve transversal polarised W^+ bosons is caused by the left-handed $u\bar{d}$ boson production [28], due to angular momentum conservation and coupling of the W^+ boson. The right-handed polarisation mode's cross section has a matrix element proportional to $(1-\cos\theta_{e^+})^2$[4], which is why it dominates the positive area, compared to the other two polarisation modes. The matrix element for the longitudinal polarised mode is proportional to $\sin^2\theta_{e^+}$[4], causing the symmetrical shape of these distributions.

The height of the distribution resembles the order of the integrated cross sections. This is not limited to the order. When comparing polarisation modes to their LAB or CM frame

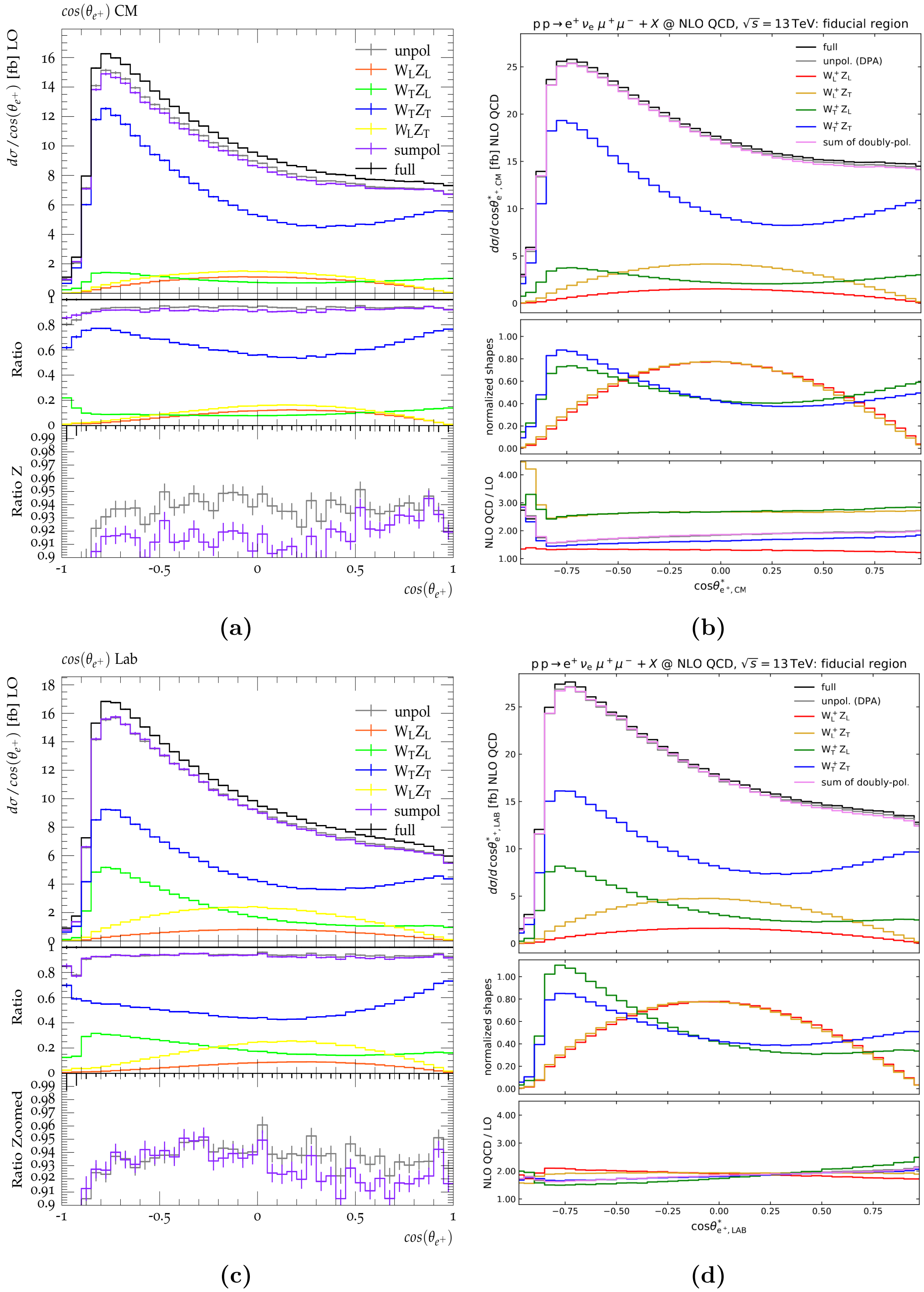

Figure 4.1: Distributions in $\cos\theta_{e^+}$ in the CM frame (a,b) and Lab (c,d) frame for NWA (a,c) and DPA (b,d). The decay angle is the positron angle in the W^+-boson rest frame with respect to the W^+-boson vector in the corresponding frame. Ration plots of NWA are in reference to the full differential XS

counterparts. The LAB frame non TT modes are comparatively higher than their counterparts, while the TT is considerably lower than its LAB frame equivalent. There is no significant difference in shape for both frames.

While figure 4.1 contained highly asymmetrical plots, this is not the case for figure A.2. The Z boson couples on particles regardless of their chiral particle states and therefore its plots are near symmetric. Both decay products have applied cuts, which results in sharp decreases on both ends of the distribution for modes including a transversal boson. It is likely that longitudinal dXS are to small for these angles. The agreement seen in the previous figure between both approximations is largely confirmed. Notice that the LAB frame has a very constant NLO/LO ratio that is nearly equal for all modes, while the LAB ratios are constant but diverse.
The distribution does not perfectly resemble their significant frame counterpart, however. The LAB graph is slightly asymmetrical for all modes that contain the TT mode. When looking at the right-handed and left-handed distributions (Appendix A.5 one can see that for left-handed W^+ bosons and right-handed Z bosons), there are significantly higher dXS in their distributions, with shapes as predicted by figure 2.5. The already mentioned higher abundance of left-handed W^+ bosons causes this. Conversation favours the mixed TT modes heavily, causing an asymmetrical distribution that is much more present in the LAB frame due to its higher TT dXS compared to the other polarisation modes. Additionally, the LAB graph has a local minimum at $\cos\theta_{\mu+} = 0$, while the LAB has a local maximum at the same position. The minima of the CM frame are likely caused by the smaller longitudinal distributions that would balance out the minimum with their maximum. The LAB frame longitudinal distributions are high enough to provide compensation.

The resembling of the NWA to the DPA plots continues in figure 4.3. When considering the shapes for the LO NWA, which are flatter than their NLO DPA equivalent, one must pay attention to the NLO/LO ratio plot to understand this. There are two major differences between CM and LAB, the TL and LT distributions. LT, TL and LL have almost the same curve for the CM frame definition. The LAB frame definition however produces a TL curve that has, in contrary to every other distribution in CM and LAB frame, a minimum at $y_{e^+} = 0$ and increases to both sides. The LT distribution has a maximum there, but it has a significantly higher slope. By comparing heights of the distribution one can recognize the same order of modes as for the integrated XS, this does extend to the CM frame having a less diverse distribution amongst its modes. The TT is comparatively higher than any other mode, while the non-TT LAB frame modes have noticeably higher dXS. The TT dXS is consequently lower. Full dXS, unpolarised and the sum of all polarised modes do have very similar values, which is not surprising since the rapidity is Lorentz invariant.
The cause of the behaviour of TL and LT distributions in the LAB frame is the boost that is the connection between the two frame definitions. This boost is more often than not in the

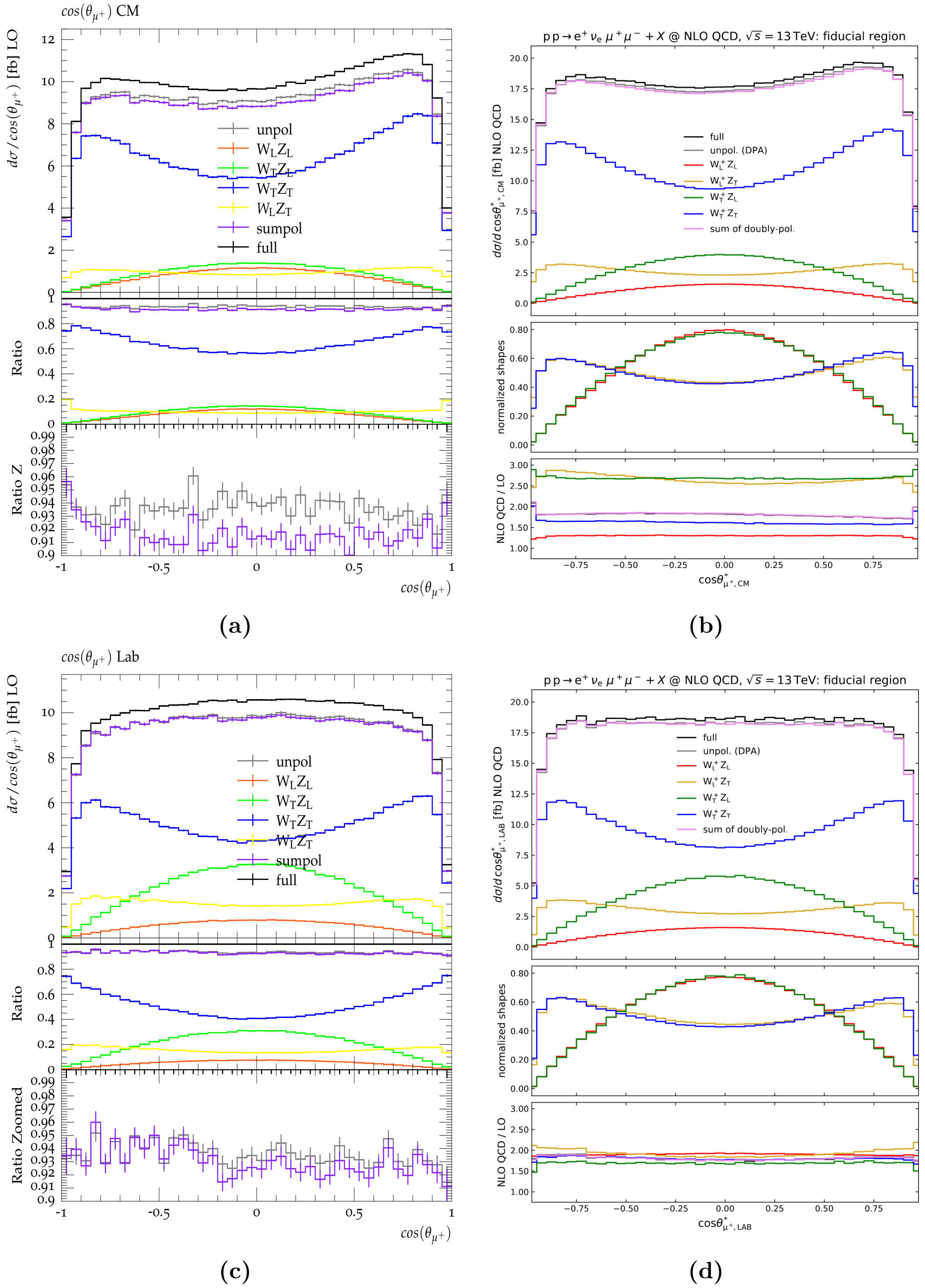

Figure 4.2: Distributions in $cos\theta_{\mu^+}$ in the CM frame (a,b) and Lab (c,d) frame for NWA (a,c) and DPA (b,d). The decay angle is the antimuon angle in the Z-boson rest frame with respect to the Z-boson vector in the corresponding frame.

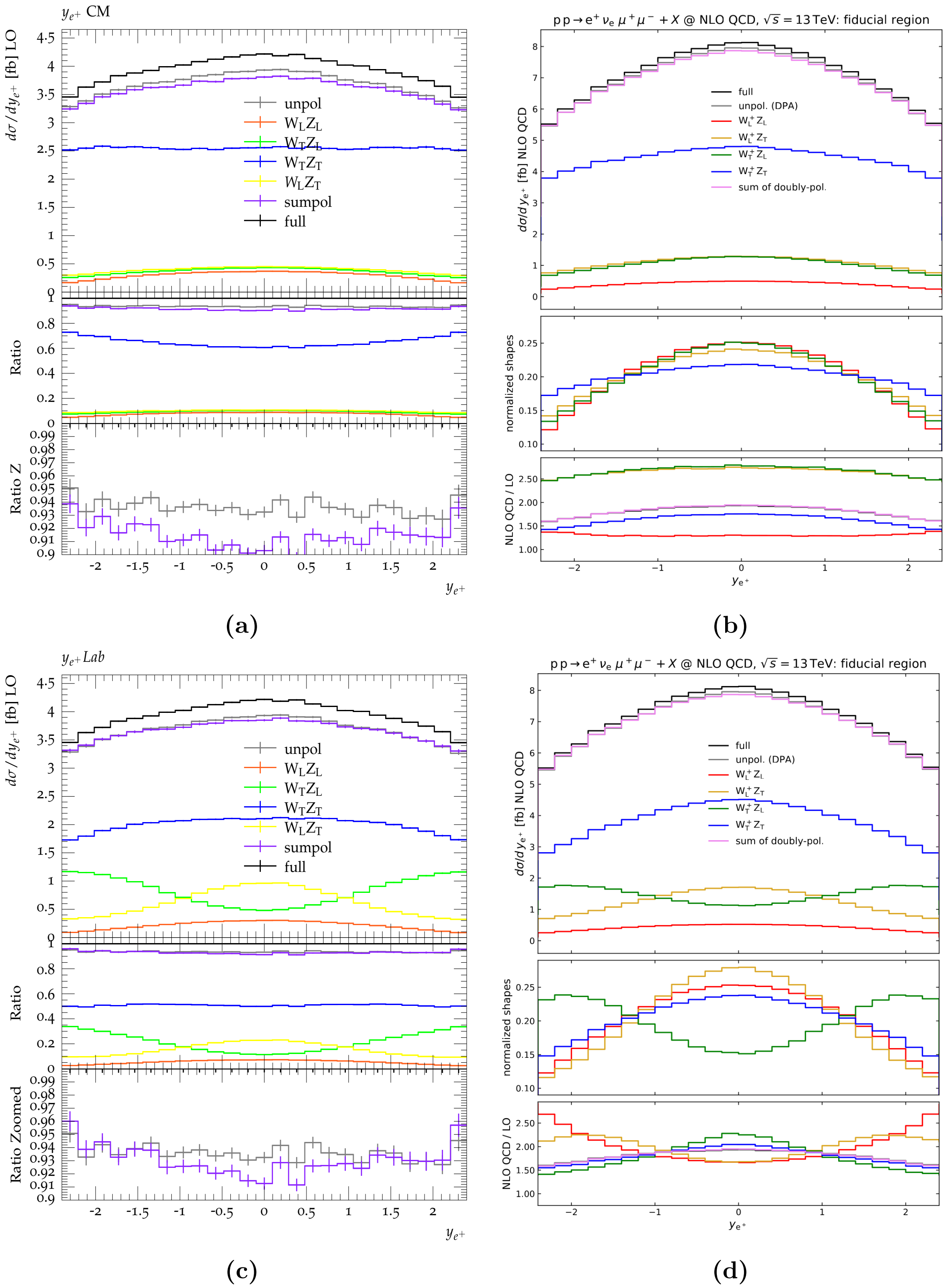

Figure 4.3: Distributions in y_{e+} in the CM frame (a,b) and LAB (c,d) frame for NWA (a,c) and DPA (b,d).

direction of u quark due to a higher PDF density than the second initial particle, the $\bar{d}$ quark. The majority of W^+-bosons in the CM frame is produced in the hemisphere of the u-quark. These two points result in a positive boost for the W^+ boson and a negative boost for the Z-boson when transitioning into the LAB frame. This negative boost can change the polarisation of the Z-boson and does so quite often. The polarisation vectors can change drastically because of their sensitivity to lowering the energy. After extreme boosts, the transversal momentum can yield the overwhelming majority in comparison to the y-axis momentum or even reverse it. This drastic change can lead to Z bosons changing their polarisation when transitioned into the LAB frame with large y_{W^+}, while the W^+ boson's polarisation remains mostly unchanged. This effect reverses for small y_{W^+} however, Z-bosons stay relatively stable while W^+-bosons change their polarisation.[11] The latter leads to transversal polarised W^+ bosons changing to a longitudinal mode for small y_{W^+}, resulting in the increased peak of LT in the LAB frame. The changing of Z polarisation at high $|y_{e^+}|$ creates the peaks or increases for the TL in LAB frame distribution. [25]

The trend of agreement between the approximations continues for the angle between the positron and the muon in figure 4.5. The NLO distribution is asymmetric, but the NLO/LO ratios, for most distributions, resemble linear increasing functions, explaining the higher peak for $\cos\theta_{e^+,\mu^-} = 1$. The distributions deviating from this general trend are LAB frame TL and LT modes, which have negative sloped linear ratios, causing a higher maximum on the positive side than what can be found for their NWA counterparts. There is one anomaly, the ratio of LL in the LAB frame has a peak at $\cos\theta_{e^+,\mu^-} = 1$ that can not be seen in the NWA LAB frame. The TT modes of both polarisation definitions have peaks at the negative and positive end of the graph. Causing this is the tendency of decay products to have their initial bosons momentum direction or the reversed version of it when the helicity of the boson is ± 1.
When boosting the boson into the LAB frame and reversing its p_z in the process, this does result in a small angle between both bosons. When both bosons have similar momentum directions, their decay products will inherit this attribute and therefore will have a small angle between them too. This results in a more diverse LAB frame distribution, while the TT in the CM frame holds the large majority. [25]

The last reviewed variable is the azimuthal angle difference between the muon and the positron in figure 4.5. Overall, these plots are relatively monotonous. All resemble a more or less linear function with a positive slope, which agrees with the ratio and NLO QCD distributions of the DPA. The LL modes have a slightly higher slope than any mode with a transversely polarised boson. An interesting observation can be made by taking a look at the interference. For the first time, we can see significant negative interference for $\Delta\phi_{e^+,\mu^-} < \pi/2$. This does result from the lepton cuts. Specifically, when integrating over the whole range of ϕ the interference vanishes. [11] The cuts limit the range and therefore interference occurs when approaching the edge of the interval.

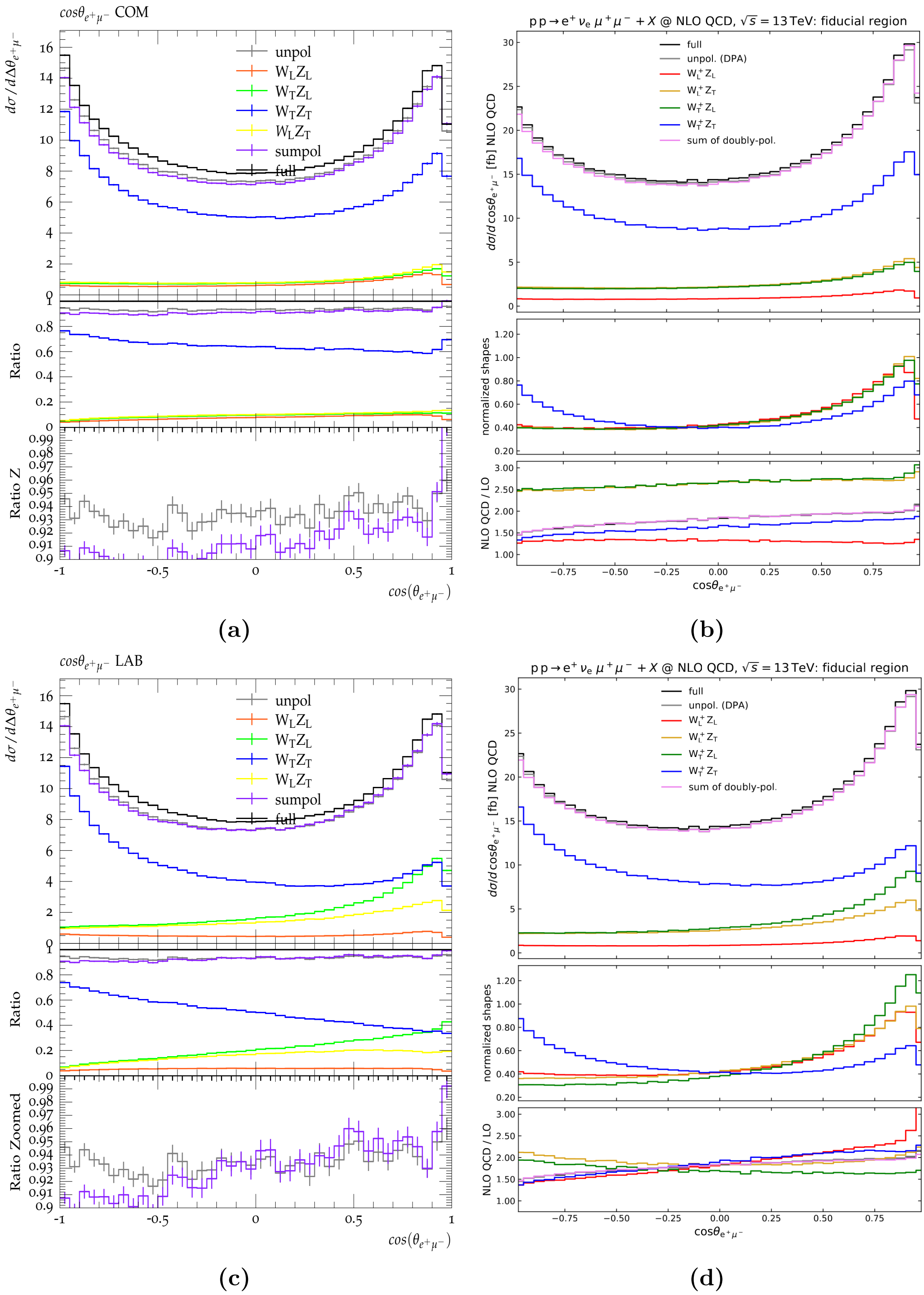

Figure 4.4: Distributions in $\cos\theta_{e^+,\mu^-}$ in the CM frame (a,b) and LAB (c,d) frame for NWA (a,c) and DPA (b,d).

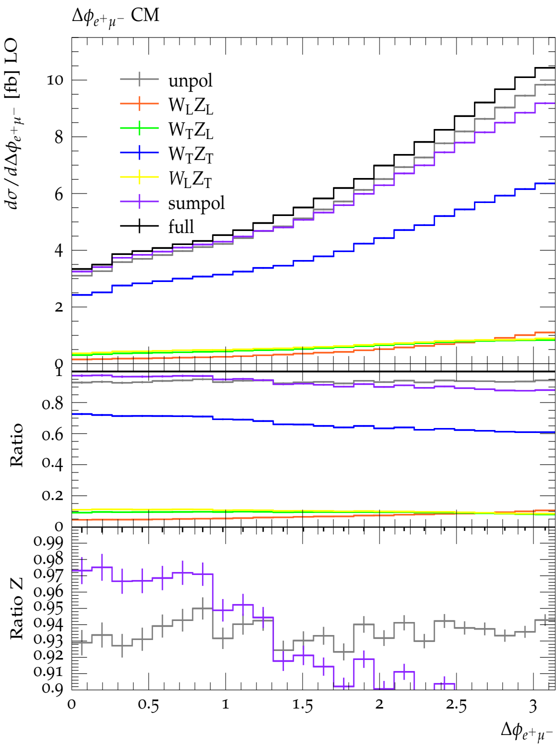

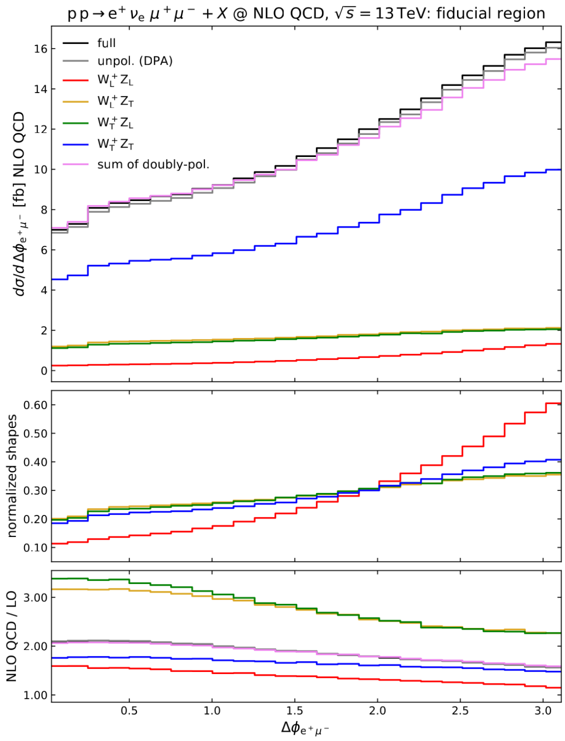

(a) **(b)**

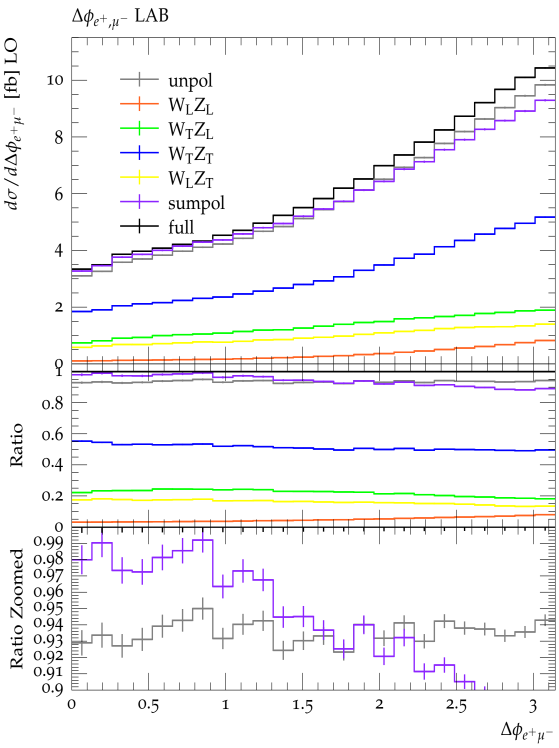

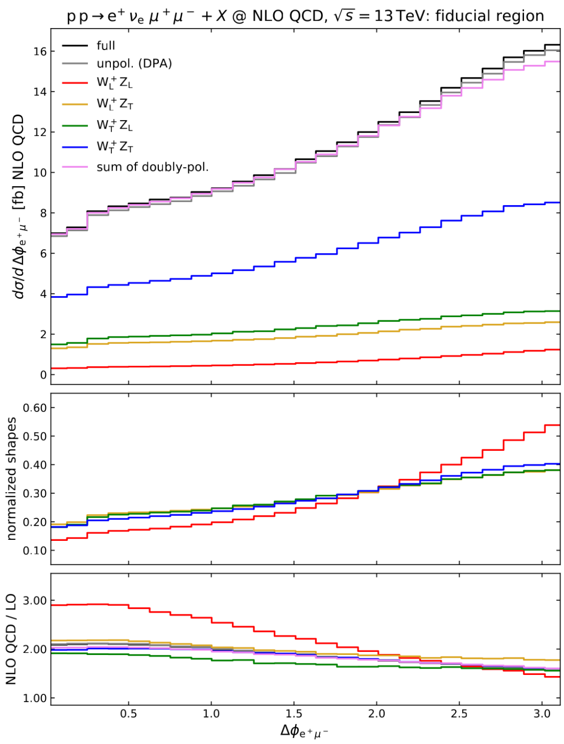

(c) **(d)**

Figure 4.5: Distributions in $\Delta\phi_{e^+,\mu^-}$ in the CM frame (a,b) and LAB (c,d) frame for NWA (a,c) and DPA (b,d).

5 Summary and Outlook

This thesis compared two implementations of polarised $W^{\pm}$ and Z bosons in two different Monte Carlo event generators. The aim was to verify the in Sherpa implemented definition and explain eventual differences. The agreement is necessary since the investigation of longitudinally polarised bosons could provide new leads to Beyond Standard Model physics or lead to an improved understanding of Electroweak Symmetry Breaking.

Both polarisation implementations use approximations. Sherpa uses the narrow-width approximation, which was displayed in detail. The comparison approximation is the doubly-pole approximation with no need to be studied in depth since its purpose was to provide verification values. Both definitions for polarisation were investigated. Simulations for both approximations there done with cuts that resemble a detector environment. To validate the comparison itself, the agreement of both fully integrated cross sections was confirmed. The comparison showed an overall agreement, however, some parameters indicate differences between both approximations. While the fractions of the polarised mode in reference to the unpolarised cross section are consistent with the values of the double-pole approximation, the absolute value of polarised cross sections is on average 4.2% below their counterparts. However, the unpolarised cross sections deviate similarly, indicating a difference between the approximation rather than the polarisation implementations.

Investigating the kinematic variables of both approximations strengthened the agreement since no major deviation could be found. The interference and the non-resonant background were higher than expected, in particular the non-resonant background for being $5\% - 10\%$. Otherwise, the kinematics observed proved to be sensitive to the different polarisation modes and suited for comparison.

The next steps could be to simulate and analyse the next-to-leading order processes involving Quantum Chromo Dynamics for a comparison to the double-pole approximation. Another direction would be investigating further processes.

A Appendix

A.1 SHERPA Full Process Runcard

```
# Sherpa configuration for W^{+-} Z full XS production
# set up beams for LHC run 2
BEAMS: 2212
BEAM_ENERGIES: 6500
# matrix-element calculation
ME_GENERATORS:
- Comix
- Amegic
# Switch off multiparton interactions
MI_HANDLER: None  # Amisic
# SCALES: VAR{sqr(90.0)}
SCALES: VAR{sqr((80.351971594+91.153480619)/2)} #oder M_W
# pp -> e, v_e, mu-, mu+
PROCESSES:
- 93 93 -> -11 12  13 -13:
    Order: {QCD: 0, EW: 4}
    Print_Graphs: Graphs
SELECTORS:
- VariableSelector:
    Variable: m
    Flavs: [13, -13]
    Ranges:
    - [81, 101]
- VariableSelector:
    Variable: PT
    Flavs: -11
    Ranges:
    - [20, E_CMS]
- VariableSelector:
    Variable: PT
    Flavs: -13
    Ranges:
    - [15, E_CMS]
- VariableSelector:
    Variable: PT
    Flavs: 13
```

```
    Ranges:
    - [15, E_CMS]
- VariableSelector:
    Variable: y
    Flavs: -11
    Ranges:
    - [-2.5, 2.5]
- VariableSelector:
    Variable: y
    Flavs: -13
    Ranges:
    - [-2.5, 2.5]
- VariableSelector:
    Variable: y
    Flavs: 13
    Ranges:
    - [-2.5, 2.5]
- VariableSelector:
    Variable: Calc(sqrt(sqr(DEta(p[0], p[1]))+sqr(DPhi(p[0], p[1]))) > 0.2)
    Flavs: [13, -13]
    Ranges:
    - [1,1]
- VariableSelector:
    Variable: Calc(sqrt(sqr(DEta(p[0], p[1]))+sqr(DPhi(p[0], p[1]))) > 0.3)
    Flavs: [-11, 13]
    Ranges:
    - [1,1]
- VariableSelector:
    Variable: Calc(sqrt(sqr(DEta(p[0], p[1]))+sqr(DPhi(p[0], p[1]))) > 0.3)
    Flavs: [-11, -13]
    Ranges:
    - [1,1]
- VariableSelector:
    Variable: Calc:(sqrt(2.0*PPerp(p[0])*PPerp(p[1])*(1-cos(DPhi(p[0], p[1])))) > 30)
    Flavs: [-11, 12]
    Ranges:
    - [1,1]
# Switch off Shower generator
SHOWER_GENERATOR: None
# no hadronisation
FRAGMENTATION: None
# switch off QED corrections
ME_QED: {ENABLED: false}
# matrix-element calculation
# BEAM_REMNANTS do not work without showers
BEAM_REMNANTS: false
PDF_LIBRARY: LHAPDFSherpa
PDF_SET: NNPDF31_lo_as_0118
```

```
ALPHAS: {USE_PDF: 1}
EW_scheme: Gmu
GF: 0.0000116638
GMU_CMS_AQED_CONVENTION: 4
EVENT_GENERATION_MODE: Weighted
PARTICLE_DATA:
  24:
    Width: 2.084298894
    Mass: 80.351971594
# source https://arxiv.org/pdf/2006.14867.pdf
  23:
    Width: 2.494266379
    Mass: 91.153480619
YFS:
    MODE: None
EVENTS: 500000
HARD_DECAYS:
    QED_Corrections: 0
ANALYSIS: Rivet
RIVET:
  -analyses:
    - MC_WZ_polar
  -ignore-beams: 1

```

A.2 SHERPA Polarised Process Runcard

```
# Sherpa configuration for W^+Z polarised XS production
# set up beams for LHC run 2
BEAMS: 2212
BEAM_ENERGIES: 6500
# matrix-element calculation
ME_GENERATORS:
#- Comix
- Amegic
# Switch off multiparton interactions
MI_HANDLER: None  # Amisic
SCALES: VAR{sqr((80.351971594+91.153480619)/2)} #oder M_W
# pp -> e, v_e, mu-, mu+
PROCESSES:
- 94 94 -> 24 23:
    Order: {QCD: 0, EW: 2}
    Print_Graphs: Graphs
#Switch off Shower generator
SHOWER_GENERATOR: None
# no hadronisation
```

```
FRAGMENTATION: None
# switch off QED corrections
ME_QED: {ENABLED: false}
# matrix-element calculation
# BEAM_REMNANTS do not work without showers
BEAM_REMNANTS: false
PDF_LIBRARY: LHAPDFSherpa
PDF_SET: NNPDF31_lo_as_0118
ALPHAS: {USE_PDF: 1}
EW_scheme: Gmu
GF: 0.0000116638
GMU_CMS_AQED_CONVENTION: 4
EVENT_GENERATION_MODE: Weighted
PARTICLE_DATA:
  24:
    Width: 0
    Mass: 80.351971594
  23:
    Width: 0
    Mass: 91.153480619
YFS:
    MODE: None
COMIX_DEFAULT_GAUGE: 0
EVENTS: 250000
HARD_DECAYS:
    Enabled: True
    Mass_Smearing: 1
    QED_Corrections: 0
    Channels:
      23,13,-13: {Status: 2}
      24,12,-11: {Status: 2}
POL_CROSS_SECTION:
    Enabled: True
    Spinbasis: Helicity
    Referencesystem: [Lab, COM]
ANALYSIS: Rivet
RIVET:
  -analyses:
    - MC_WZ
  -ignore-beams: 1
```

A.3 Rivet Analysis

```
// -*- C++ -*-
#include "Rivet/Analysis.hh"
#include "Rivet/Projections/WFinder.hh"
#include "Rivet/Projections/ZFinder.hh"
#include "Rivet/Math/LorentzTrans.hh"
#include "Rivet/Projections/VetoedFinalState.hh"
#include "Rivet/Projections/DressedLeptons.hh"
#include "Rivet/Projections/PromptFinalState.hh"

namespace Rivet {

  class W_candidate{
  public:
    W_candidate() {};

    FourMomentum momentum() const {
      return candidate.first.mom() + candidate.second.mom();
       };

      double inv_mass() {
              return (candidate.first.mom() + candidate.second.mom()).mass();
      };

      double W_mass_window() {
              return fabs((candidate.first.mom() + candidate.second.mom()).mass() - 80.379);
      };

      void make_W_candidate(Particle lepton, Particle neutrino) {
        candidate = std::make_pair(lepton, neutrino);
      };

          Particle lepton() {return candidate.first;};
          Particle neutrino(){return candidate.second;};
          ParticlePair candidate;
  };

  /// @brief MC validation analysis for W^+- Z events
  class MC_WZ_pol : public Analysis {
  public:

      /// Default constructor
      MC_WZ_pol()
        : Analysis("MC_WZ_pol")
      {   }

```

```
    /// @name Analysis methods
    //@{

    /// Book histograms
    void init() {
            FinalState fs;
      Cut cutz = Cuts::pT > 0*GeV; //Cuts::abseta < 2.5 &&
      IdentifiedFinalState el_id(fs);
      el_id.acceptIdPair(PID::ELECTRON);
      declare(el_id, "Electrons");

      IdentifiedFinalState ifsNeutrinos({12});
      declare(ifsNeutrinos, "projNeutrinos");

      FinalState zmminput;
      ZFinder zmmfinder(zmminput, cutz, PID::MUON,
          0*GeV, 13000*GeV, 0.2, ZFinder::ClusterPhotons::NODECAY,
          ZFinder::AddPhotons::YES);
      declare(zmmfinder, "ZmmFinder");

      // Properties of the Z bosons
      book(_h_Z_costheta_Lab, "Z_costheta_Lab", 40, -1.0, 1.0);
      book(_h_Z_costheta_CM, "Z_costheta_CM", 40, -1.0, 1.0);

      // properties of the W bosons
      book(_h_W_eta ,"W_eta", 25, -2.4, 2.4);
      book(_h_W_costheta_Lab, "W_costheta_Lab", 40, -1.0, 1.0);
      book(_h_W_costheta_CM, "W_costheta_CM", 40, -1.0, 1.0);


      // cross sections and Positron-Muon properties
      book(_h_WZ_XS, "WZ_XS", 1, 0, 1);
      book(_h_PM_theta,"PM_theta", 40, -1.0, 1.0);
      book(_h_PM_dphi, "PM_dphi",24,0, PI);

    }
    // Boosting and Rotating leptons in LAB and CM Frames with
    // given Lorentz- Boosts, in this case bosons
    Vector3 BoostAndRotate_LabFr(const FourMomentum m_boost, const FourMomentum m_momentum) {
          const LorentzTransform m_transform
              = LorentzTransform::mkObjTransformFromBeta(-(m_boost.betaVec()));
          Matrix3 l_zrot(m_boost.vector3(), Vector3(0.0, 0.0, 1.0));
          return l_zrot*(m_transform.transform(m_momentum).vector3());
      }


           Vector3 BoostAndRotate_WZRFr(const FourMomentum boson1, const FourMomentum boson2,
              const FourMomentum momentum) {
```

```
            // boosting into COM frame
            const LorentzTransform transformBoson12
                = LorentzTransform::mkObjTransformFromBeta(-((boson1+boson2).betaVec()));
            const LorentzTransform  transformBoson1
                = LorentzTransform::mkObjTransformFromBeta(
                    -(transformBoson12.transform(boson1).betaVec()));
            Matrix3 l_zrot(transformBoson12.transform(boson1).vector3(),
                    Vector3(0.0, 0.0, 1.0));
            return l_zrot*(transformBoson1.transform(
                transformBoson12.transform(momentum)).vector3());
        }



      /// Do the analysis
      void analyze(const Event& event) {

        const Particles neutrinos
            = apply<IdentifiedFinalState>(event, "projNeutrinos").particles();

        if (neutrinos.size() != 1) vetoEvent;
        Particle neutrino = neutrinos[0];
        Particles positrons = apply<IdentifiedFinalState>(event, "Electrons").particles();
        if (positrons.size() != 1) vetoEvent;
        Particle positron = positrons[0];
        W_candidate W;
        W.make_W_candidate(positron, neutrino);

        const ZFinder& zmmfinder = apply<ZFinder>(event, "ZmmFinder");
        if (zmmfinder.bosons().size() != 1) vetoEvent;

        const FourMomentum& zmm = zmmfinder.bosons()[0].momentum();
        const FourMomentum wenu = W.momentum();
        const FourMomentum wz = wenu + zmm;
        const FourMomentum wenu_l = W.lepton().momentum();
        const FourMomentum wenu_n = W.neutrino().momentum();
        const FourMomentum zmm_l1 = zmmfinder.constituentLeptons()[0].momentum();
        const FourMomentum zmm_l2 = zmmfinder.constituentLeptons()[1].momentum();

        // apply cuts
         if (zmmfinder.constituentLeptons().size() != 2) vetoEvent;
         if (wenu_l.pT() <= 20*GeV) vetoEvent;
         if (zmm_l1.pT() <= 15*GeV) vetoEvent;
         if (zmm_l2.pT() <= 15*GeV) vetoEvent;
         if (wenu_l.absrap() >= 2.5) vetoEvent;
         if (zmm_l1.absrap() >= 2.5) vetoEvent;
         if (zmm_l2.absrap() >= 2.5) vetoEvent;
         if (sqrt(2*wenu_l.pT()*wenu_n.pT()*(1-cos(deltaPhi(wenu_l, wenu_n)))) <= 30*GeV)
```

```
          vetoEvent;
       if (sqrt(sqr(deltaEta(wenu_l, zmm_l1))+sqr(deltaPhi(wenu_l, zmm_l1))) <= 0.3)
          vetoEvent;
       if (sqrt(sqr(deltaEta(wenu_l, zmm_l2))+sqr(deltaPhi(wenu_l, zmm_l2))) <= 0.3)
          vetoEvent;
       if (sqrt(sqr(deltaEta(zmm_l1, zmm_l2))+sqr(deltaPhi(zmm_l1, zmm_l2))) <= 0.2)
          vetoEvent;
       if ((zmm_l2 + zmm_l1).mass() <= 81*GeV || (zmm_l2 + zmm_l1).mass() >= 101*GeV)
          vetoEvent;

      // calculating  cos \theta
      Vector3 wenu_l_WF = BoostAndRotate_LabFr(wenu, wenu_l);
      double costheta_W_Lab = cos(wenu_l_WF.theta());

      Vector3 zmm_l_ZF = BoostAndRotate_LabFr(zmm, zmm_l1);
      double costheta_Z_Lab = cos(zmm_l_ZF.theta());

      Vector3 wenu_l_WZF = BoostAndRotate_WZRFr(wenu, zmm, wenu_l);
      double costheta_W_CM = cos(wenu_l_WZF.theta());

      Vector3 zmm_l_WZF = BoostAndRotate_WZRFr(zmm, wenu, zmm_l1);
      double costheta_Z_CM = cos(zmm_l_WZF.theta());

      // filling histogram
      _h_W_eta->fill(wenu_l.rap());
      _h_W_costheta_Lab->fill(costheta_W_Lab);
      _h_Z_costheta_Lab->fill(costheta_Z_Lab);
      _h_W_costheta_CM->fill(costheta_W_CM);
      _h_Z_costheta_CM->fill(costheta_Z_CM);
      _h_PM_theta -> fill(cos(zmm_l2.angle(wenu_l)));
      _h_PM_dphi -> fill(deltaPhi(zmm_l2, wenu_l));
      _h_WZ_XS -> fill(0.5);
    }

    /// Finalize
    void finalize() {
      const double norm = crossSection()/femtobarn/sumOfWeights();
      std::cout << crossSection();
      scale(_h_W_eta, norm);
      scale(_h_W_costheta_Lab, norm);
      scale(_h_Z_costheta_Lab, norm);
      scale(_h_W_costheta_CM, norm);
      scale(_h_Z_costheta_CM, norm);
      scale(_h_WZ_XS, norm);
      scale(_h_PM_theta, norm);
      scale(_h_PM_dphi, norm);
      //std::cout << "final";
    }
```

```
      //@}

  private:
    /// @name Histograms
    //@{
    Histo1DPtr _h_W_eta;
    Histo1DPtr _h_W_costheta_Lab;
    Histo1DPtr _h_Z_costheta_Lab;
    Histo1DPtr _h_W_costheta_CM;
    Histo1DPtr _h_Z_costheta_CM;
    Histo1DPtr _h_WZ_XS;
    Histo1DPtr _h_PM_theta;
    Histo1DPtr _h_PM_dphi;
    //@}^
  };


 // The hook for the plugin system
 RIVET_DECLARE_PLUGIN(MC_WZ_pol);
}
```

A.4 SHERPA Feynman Graph Output

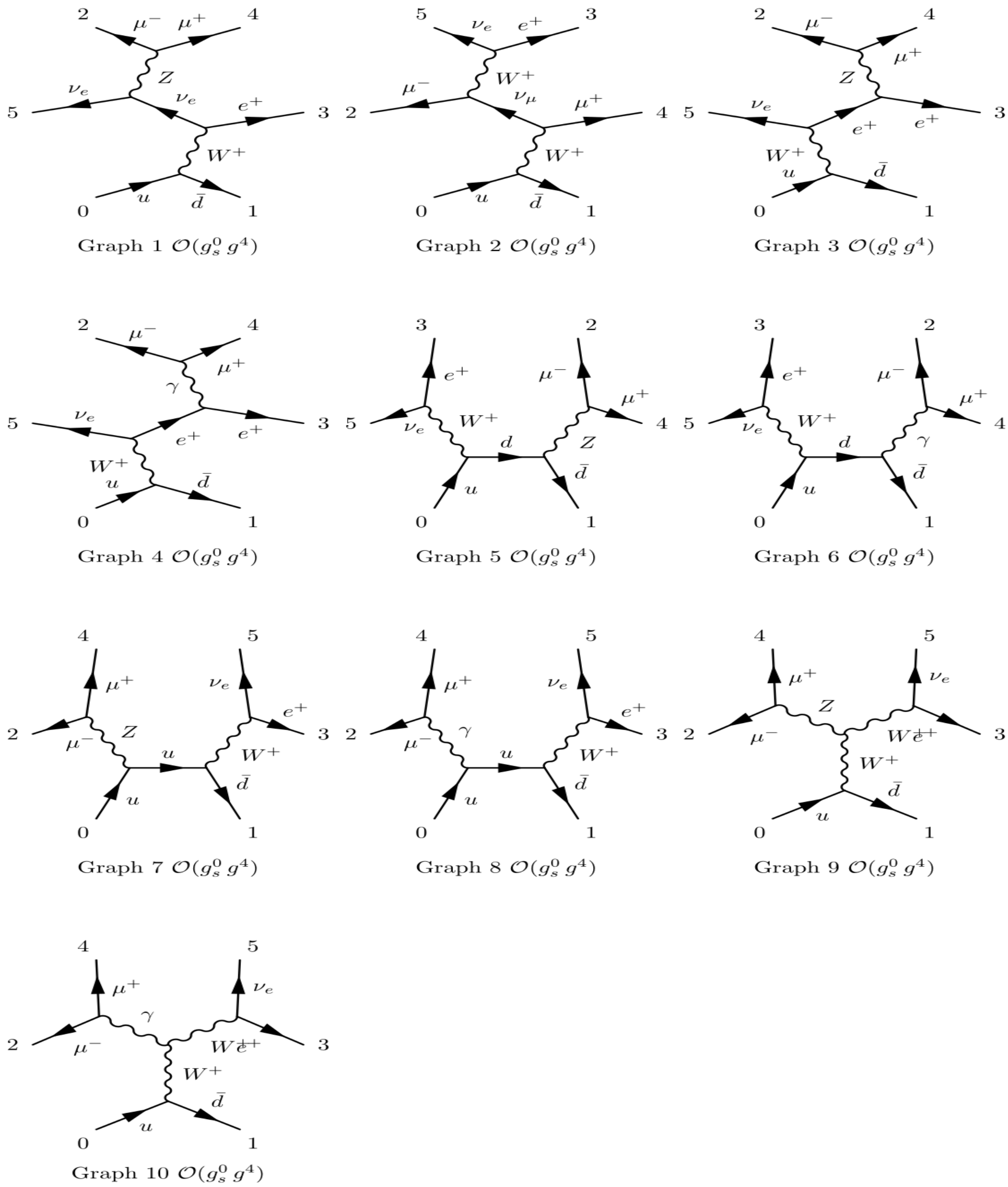

Figure A.1: Feynamn Graphs output by SHERPA for the total cross-section runcard

A.5 Muon Decay Angle for right- and left-handed Modes

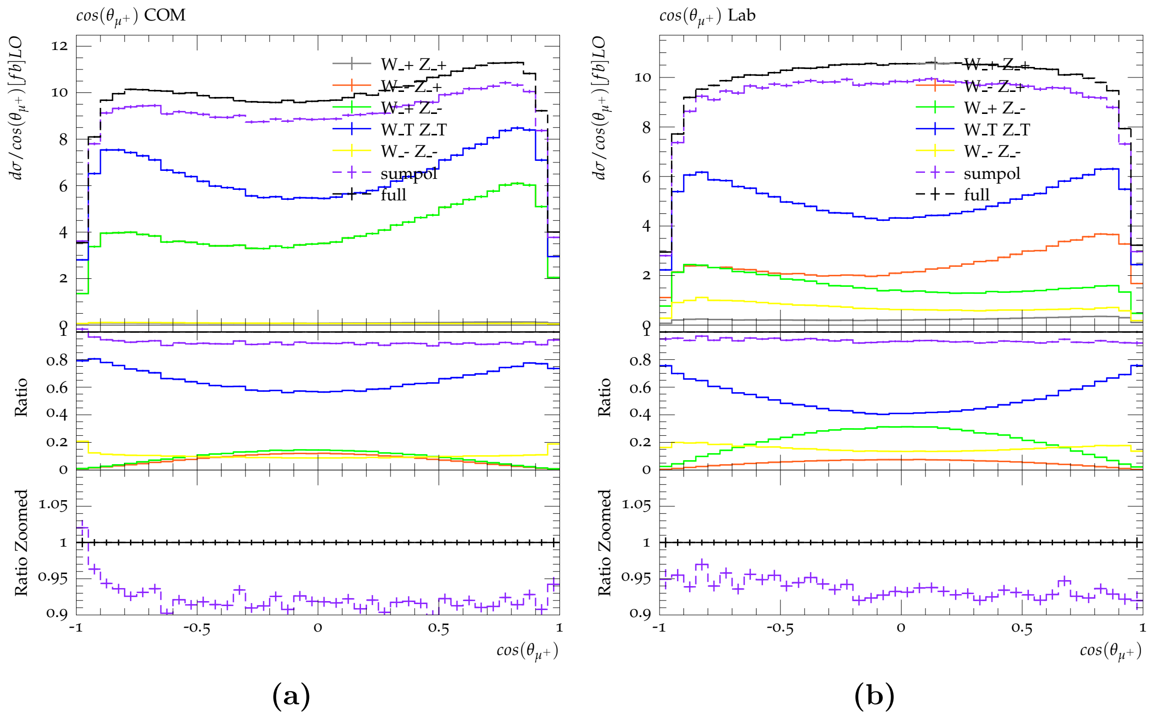

Figure A.2: Distributions in $\cos\theta_{\mu^+}$ in the Centre-of-Mass frame (a) and Lab (b) frame for NWA. The decay angle is the antimuon angle in the Z-boson rest frame with respect to the Z-boson vector in the corresponding frame. The transversal polarisation mode has been split up into right-(+) and left-handed(-) polarisation modes.

B Bibliography

[1] T. McEvilley. *The Shape of Ancient Thought: Comparative Studies in Greek and Indian Philosophies*. Aesthetics Today Series. Allworth Press, 2002.

[2] J. J. Thomson M.A. F.R.S. Xl. cathode rays. *The London, Edinburgh, and Dublin Philosophical Magazine and Journal of Science*, 44(269):293–316, 1897. URL: `https://doi.org/10.1080/14786449708621070`.

[3] ATLAS Collaboration. Observation of a new particle in the search for the standard model higgs boson with the ATLAS detector at the LHC. *Physics Letters B*, 716(1):1–29, sep 2012. URL: `https://doi.org/10.1016%2Fj.physletb.2012.08.020`.

[4] Mark Thomson. *Modern particle physics*. Cambridge University Press, New York, 2013.

[5] Robert Mann. *An Introduction to Particle Physics and the Standard Model*. CRC Press, Boca Raton, 2010.

[6] ATLAS Collaboration. Study of the spin and parity of the higgs boson in diboson decays with the ATLAS detector. *The European Physical Journal C*, 75(10), oct 2015. URL: `https://doi.org/10.1140%2Fepjc%2Fs10052-015-3685-1`.

[7] Daniel Naegels. An introduction to goldstone boson physics and to the coset construction, 2021. URL: `https://arxiv.org/abs/2110.14504`.

[8] A. Pich. Electroweak symmetry breaking and the higgs boson. *Acta Physica Polonica B*, 47(1):151, 2016. URL: `https://doi.org/10.5506%2Faphyspolb.47.151`.

[9] Mareen Hope. Implementation of polarized cross sections for vector boson production in sherpa. Warb-Presentation, 2022.

[10] Cheng-Yang Lee. Spin and helicity of massive particles, 2016. URL: `https://arxiv.org/abs/1607.05370`.

[11] Ansgar Denner and Giovanni Pelliccioli. Polarized electroweak bosons in ww- production at the LHC including NLO QCD effects. *Journal of High Energy Physics*, 2020(9), sep 2020. URL: `https://doi.org/10.1007%2Fjhep09%282020%29164`.

[12] CERN: LHC run 3 record energy starts tomorrow. https://home.cern/news/news/physics/lhc-run-3-physics-record-energy-starts-tomorrow. Accessed: 2022-12-18.

[13] J M Campbell, J W Huston, and W J Stirling. Hard interactions of quarks and gluons: a primer for LHC physics. *Reports on Progress in Physics*, 70(1):89–193, dec 2006. URL: https://doi.org/10.1088%2F0034-4885%2F70%2F1%2Fr02.

[14] Carsten Bittrich. Study of Polarization Fractions in the Scattering of Massive Gauge Bosons $W^{\pm}Z \to W^{\pm}Z$ with the ATLAS Detector at the Large Hadron Collider. Master's thesis, Dresden, Tech. U., 4 2015.

[15] Michelangelo L. Mangano and Timothy J. Stelzer. Tools for the simulation of hard hadronic collisions. *Annual Review of Nuclear and Particle Science*, 55(1):555–588, 2005. URL: https://doi.org/10.1146/annurev.nucl.55.090704.151505.

[16] Enrico Bothmann et al. Event generation with sherpa 2.2. *SciPost Physics*, 7(3), sep 2019. URL: https://doi.org/10.21468%2Fscipostphys.7.3.034.

[17] Andy Buckley et al. General-purpose event generators for LHC physics. *Physics Reports*, 504(5):145–233, jul 2011. URL: https://doi.org/10.1016%2Fj.physrep.2011.03.005.

[18] Johan Alwall, Michel Herquet, Fabio Maltoni, Olivier Mattelaer, and Tim Stelzer. MadGraph 5: going beyond. *Journal of High Energy Physics*, 2011(6), jun 2011. URL: https://doi.org/10.1007%2Fjhep06%282011%29128.

[19] Alessandro Ballestrero, Aissa Belhouari, Giuseppe Bevilacqua, Vladimir Kashkan, and Ezio Maina. PHANTOM: A monte carlo event generator for six parton final states at high energy colliders. *Computer Physics Communications*, 180(3):401–417, mar 2009. URL: https://doi.org/10.1016%2Fj.cpc.2008.10.005.

[20] J. Reuter, F. Bach, B. Chokoufe Nejad, W. Kilian, T. Ohl, M. Sekulla, and C. Weiss. Modern particle physics event generation with whizard, 2014. URL: https://arxiv.org/abs/1410.4505.

[21] D. Berdine, N. Kauer, and D. Rainwater. Breakdown of the narrow width approximation for new physics. *Physical Review Letters*, 99(11), sep 2007. URL: https://doi.org/10.1103%2Fphysrevlett.99.111601.

[22] Peter Richardson. Spin correlations in monte carlo simulations. *Journal of High Energy Physics*, 2001(11):029–029, nov 2001. URL: https://doi.org/10.1088%2F1126-6708%2F2001%2F11%2F029.

[23] Rivet Hepforge. https://rivet.hepforge.org. Accessed: 2022-12-18.

[24] Maree [preliminary Hoppe. Implementation and Phenomenology of polarized cross sections in the simulation of vector boson production with the Sherpa event generator. Master's thesis, Dresden, Tech. U., 3 2023.

[25] Ansgar Denner and Giovanni Pelliccioli. NLO QCD predictions for doubly-polarized WZ production at the LHC. *Physics Letters B*, 814:136107, mar 2021. URL: `https://doi.org/10.1016%2Fj.physletb.2021.136107`.

[26] ATLAS Collaboration. Measurement of $w^{\pm}z$ production cross sections and gauge boson polarisation in pp collisions at $\sqrt{s} = 13\,Tev$ with the ATLAS detector. *The European Physical Journal C*, 79, jun 2019. URL: `https://doi.org/10.1140%2Fepjc%2Fs10052-019-7027-6`.

[27] Sherpa Team. Sherpa manual release 3.0.0alpha1, 2022.

[28] Z. Bern, G. Diana, L. J. Dixon, F. Febres Cordero, D. Forde, T. Gleisberg, S. Höche, H. Ita, D. A. Kosower, D. Maître, and K. Ozeren. Left-handed w bosons at the LHC. *Physical Review D*, 84(3), aug 2011. URL: `https://doi.org/10.1103%2Fphysrevd.84.034008`.

Erklärung

Hiermit erkläre ich, dass ich diese Arbeit im Rahmen der Betreuung am Institut für Kern- und Teilchenphysik ohne unzulässige Hilfe Dritter verfasst und alle Quellen als solche gekennzeichnet habe.

Jannes Liersch
Dresden, Dezember 2022